國立交通大學

電機資訊學院

光電工程研究所

碩士論文

表面穩定強誘電性液晶之隨機過程

Stochastic Reorientation Processes of Defect-Free Surface-Stabilized Ferroelectric Liquid Crystal with and without Doping of ZnO nanocrystals

研 究 生：鄭綿綿

指導教授：黃中垚 教授

潘犀靈 教授

中華民國九十八年六月

表面穩定強誘電性液晶之隨機過程

研究生：**鄭綿綿**　　指導教授：**黃中垚** 教授

潘犀靈 教授

國立交通大學

光電工程研究所

摘要

在統計力學中，擾動耗散定律揭開了分子熱擾動的存在及其重要性。然而，這看似雜訊般的信號背後隱藏的資訊卻鮮為人知。本論文的主旨著重在探討特定凝態材料– 鐵電相液晶分子及其摻雜氧化鋅奈米微晶的動態行為(或稱表面穩定強誘電性液晶)。

液晶方向矢的擾動是由液晶材料特性所決定。因此本論文從液晶擾動方程與其對應的動態散射光開始，在經由探測散射光訊號的自我相關函式得到與鐵電相液晶的物理參數之相關性，並配合動態光散射實驗確認摻雜氧化鋅奈米微晶之表面穩定強誘電性液晶，其整體液晶分子排列較佳，此特徵可從熱擾動的表現改變而發覺，並可歸因於材料特性的變動;此外，摻雜氧化鋅奈米微晶之表面穩定強誘電性液晶在外加相同驅動電場下，擁有比未摻雜之強誘電性液晶元件快的反應速度。

Stochastic Reorientation Processes of Defect-Free Surface-Stabilized Ferroelectric Liquid Crystal with and without Doping of ZnO nanocrystals

Student: Mein-Mein Chang Advisors: Professor Jung Y. Huang
Professor Ci-Ling Pan

Department of Photonics and Institute of Electro-optical Engineering,

National Chiao Tung University

Abstract

The fluctuation-dissipation theorem unveils the importance of thermal molecular motion which always exists, even in thermal equilibrium, as a fluctuation. However, the underlying information of thermal fluctuation which appears to be random noise is a huge question mark that had been overlooked for years. This thesis study focuses on the discussion about the dynamics of molecular fluctuations in a specific condensed matter- the ferroelectric liquid crystals (FLC) with and without doping of nanocrystal ZnO.

The dynamics of orientation director fluctuations is governed by the material properties of the liquid crystal. In this thesis, we first derive the relation between the scattered light intensity and fluctuations of the FLC director which, through some reasonable assumption, could be described as a stochastic equation of motion. After performing autocorrelation technique to the scattered light signals, we have come to realize that the internal fluctuation is characterized by a correlation function of relevant physical quantities of the FLC system fluctuating in thermal equilibrium. The measurement results lead to the fact of improved molecular alignment and faster response time in the SSFLC cell doped with ZnO nanocrystals.

誌謝

回顧碩士班的點點滴滴，我才發覺自己非常非常的幸運，能夠給這樣博學多聞的老師們指導，並在學習的路程上，有實驗室這些可愛有趣的學長姐弟們陪伴。由衷的感謝黃老師及潘老師，老師不厭其煩的解說及每一次 meeting 的研究探討，都讓我從原本懵懂無知的菜鳥大學生，慢慢地學習成長並開始明瞭科學之浩大精深; 實驗室學姐柳萱，不管在學術上的指引，還是一般的閒話家常，學姐都讓我十分的佩服及欣賞，真的很感謝學姐一路上溫暖的支持; 還有熱心的雲漢學長，雖然相處時間稍短，但學長的真誠以及熱心讓我印象深刻; 而秉寬學長對科學的熱忱，也深深地打動我，使我能夠以一個認真的態度來面對我的研究；最不可或缺的實驗室好伙伴之程式達人阿輝，謝謝你無私的傾囊教學，讓我這麼一個程式白癡也可以開始自己寫一些小小程式，我會永遠記得一起打拼的日子; 當然不能忘記實驗室的小學弟建佑，幽默風趣的言談和對科學專業的見解，總是讓我開懷大笑又充滿佩服。

這一路上，最想感謝的是我家人。謝謝爸爸從來沒有苛責過我，總是帶給我正面樂觀的思想，教導我正確的觀念，在我因研究而陷入苦思而無法掙脫時，爸爸的鼓勵是我唯一的動力。還有我身邊許多親愛的朋友，感謝阿尼每一次耐心的教導我基本的機械概念，當我對物理意義感到不解而歇斯底里時，你總是不厭其煩地和我討論，藉此讓我得到許多新的想法。也謝謝條碼貓助教的溫馨外送香香鍋，實驗室大夥兒都讚不絕口。當然還有總是不停關切的好朋友們，亞慈，新聞，維娜，老康，星媽...，你們的打氣與加油真的溫暖了我的心。

感謝主，讓我在這些日子裡，遇到這麼多好朋友，好老師，還有不離不棄的我最愛的家人，讓我在任何時刻，尤其是傷心困頓時，都還是感覺到滿滿的幸福和快樂。感謝主!

List of Figures

Chapter 1

Introduction to the Optical and Fluctuation-Dissipation Properties of SSFLC

1.1 Motivation

Almost two centuries ago, the atomic nature of matter was elegantly revealed by Brownian motion- as exemplified by the random motion of pollen particles in water as they are bombarded by water molecules. In 1905, Albert Einstein pointed out a subtle consequence of the fluctuations in classical Brownian motion- the "fluctuation-dissipation theorem", which is one of the deepest results of thermodynamics and statistical physics. This important theorem indicates that the dynamics induced by thermal energy is not just a function of temperature, but also of many parameters that characterize the state of thermal equilibrium. To be precise, the thermodynamics is a mirror of a physical system under measure. For example, the viscosity of the fluid and the size of the suspending particles are crucial to Brownian motion; the anchoring strength of a LC cell determines the relaxation time of the corresponding autocorrelation function of thermal molecular motion. These will-established

formulas strongly imply that the thermal fluctuations may seem chaotic, irregular, and meaningless, but through a proper mathematical interpretation it would turn into some useful information, in particular for material testing. The surprising facts are something scientists have been overlooking for decades, because these fluctuations are not easily detected, and they seem harmless in magnitude. In this thesis, we attempt to probe the dynamical information out of a specific condensed matter- ferroelectric liquid crystal. This kind of material is noted for the partial molecular order that is commonly seen in some bio-tissue like RNA, protein, spindle fiber and so on. From a different point of view, knowing the information behinds the thermodynamics in liquid crystals may play an important role in exploring the human body.

This thesis is organized as follows: in chapter 1, we give a brief introduction to the fascinating material- liquid crystals; in chapter 2, we obtain a mathematical derivation in terms of thermal excitation; in chapter 3, we show the comparison between simulation and experiment results; in chapter 4, we probe how the thermal motion comes into play with an external field driven. This should be a critical issue, for the thermal energy is absolutely inevitable in a practical application; finally, we summarize our main conclusion in chapter 5.

1.2 Experiment Setup

The apparatus used for a light scattering investigation is shown in Fig. 1-2-1. It consists of a laser, the optics for polarizing and focusing the input beam, the optics for analyzing and detecting the scattered photons and the autocorrelation electronics. The laser is one of the critical modules of the set-up. First, it should provide about 5-20mW of stable power to assure that the scattered light intensity is considerable, but not to such an extent as to melt liquid crystal. Here, we use a He-Ne laser with a wavelength of 632.8 nm as an optical excitation source. The polarizers P_1 and P_2 must be arranged in a cross-polarization geometry so that the electric field component of the scattered light from the sample under study along the transmissive direction of P_2 is permitted to pass, which flickers in response to the liquid crystal molecular fluctuations. The sample is mounted into a temperature-controlled oven that is put on a rotating stage, providing an easy way to adjust the angle between the polarization of the incident light and the alignment direction of surface-stabilized ferroelectric liquid crystals. The scattered light is detected with a photomultiplier tubes (PMT) and analyzed by an autocorrelation electronics (Flex02-01E).

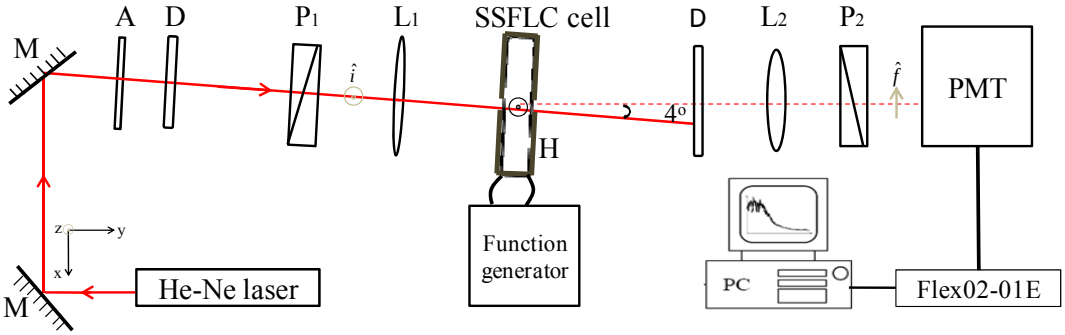

Fig. 1-2-1 Experimental setup for measuring the autocorrelation of optical scattering signal from a surface-stabilized ferroelectric liquid crystal. M: mirror; P1 and P2: polarizers; L: Lens; D: diaphragm. Here the polarization of the incoming beam $\hat{i}$ is set to be parallel to the ferroelectric liquid crystal director $\hat{n}$, but perpendicular to both the scattering plane and the polarization analyzing direction $\hat{f}$ for the output scattering beam.

In this thesis study, four kinds of surface-stabilized ferroelectric liquid crystal cells were made and measured: which are LC cells doped with 0 wt%, 0.5 wt%, 1 wt% and 5 wt% nc-ZnO, respectively. The LC used are chiral smectic C phase, meaning that they have a layered structure with the molecules tilting away from the layer normal at some angle called cone angle. This cone angle is sensitive to temperature [1], therefore we used an accurate temperature-controlled oven with ± 0.1 ℃ precision to maintain the cone angle constant in order to get a pure fluctuating conic motion.

To probe the dynamics of surface-stabilized ferroelectric liquid crystal, the thesis is then divided into two subjects: thermal fluctuations and the dynamical response to an electric field.

1.3 Optical Properties of Ferroelectric Liquid Crystal

1.3.1 The Overview of Liquid Crystal

The states of matters can be classified according to their degrees of spatial order. Briefly speaking, there are gaseous, liquid, and solid phases. However, between liquid and crystalline phases, there are mesophases and are called liquid crystals as illustrated in Fig. 1-3-1. Liquid crystals preserve a combination of properties that are associated with both liquids and crystals. Liquid crystals can be further categorized into the following three major subphases by their molecular spatial arrangement: nematic, smectic and cholesteric phases. Nematic molecules are positionally random but orientationally correlated while smectic molecules possess both orientational and positional order and tend to arrange themselves in layers. The schematic representations are shown in Fig. 1-3-1. From Fig. 1-3-2, we can see that liquid crystals molecules tend to point in the same average direction, thus yield orientational order. This preferred average direction, by definition, is called the director of liquid crystal, and is denoted by $\hat{n}$. Fig. 1-3-2 (b) and (c) are two types of smectic phase liquid crystals. They differ in their orientation of the director. The director in the smectic-A phase is parallel to the layer normal while the director in the smectic-C

phase is tilted at an angle smaller than 90° from the layer normal. As for cholesterics phase as depicted in Fig. 1-3-2 (d), the structure undergoes a helical distortion, leading to the director $\hat{n}$ not constant in space.

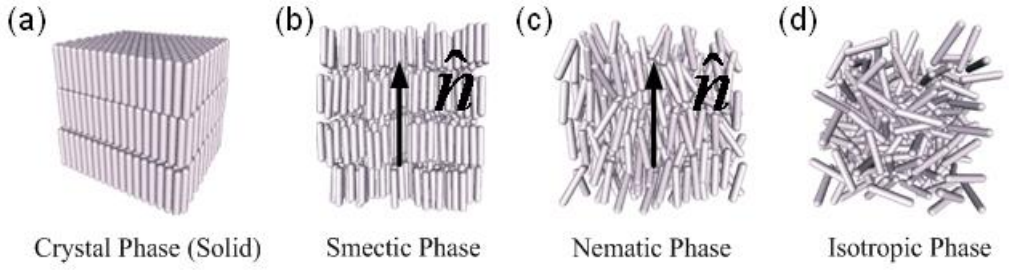

Fig. 1-3-1 The pictures from left to right are arranged in a decreasing order of spatial alignment. (a) As sketched, the molecular constituents in a solid material not only occupy periodic spatial positions, but they also orient in a specific spatial direction; (b) Smectic and (c) nematic phases belong to liquid crystalline phases but are differ in their molecular orientations and degree of order; (d) Molecules in isotropic phase are randomly distributed; $\hat{n}$ represents the director of liquid crystals.

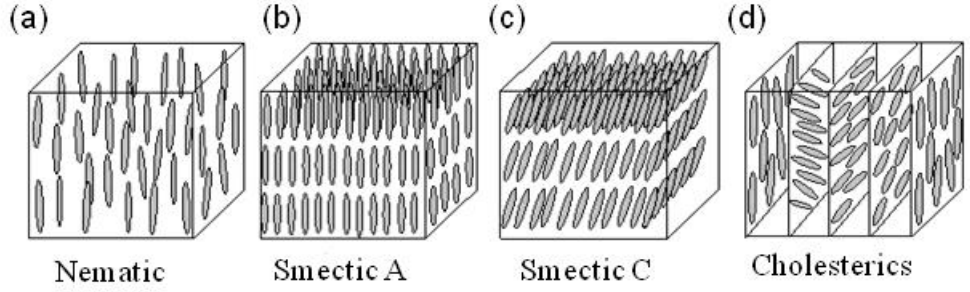

Fig. 1-3-2 The three major subphases of liquid crystal categorized by the molecular alignment: (a) the molecules in the nematic phase tend to orient towards some common axis and lead to an orientational order; (b) the molecular arrangement in the smectic A phase form a layer structure and give rise to a small degree of positional order; (c) the molecules in a smectic-C phase tilt an angle less than 90° with respect to the layer normal and also form a layer structure; (d) helical structure is the major characteristic of a cholesterics phase liquid crystal.

The terms “orientational order” as well as “positional order” that have mentioned previously are physical properties in describing a spatially ordered structure. The consequences of the orientational order in liquid crystals are most easily understood by comparing it to the positional order in solid crystals, as shown in Fig. 1-3-3. In solids, a given crystal belongs to one of the 230 space groups. These groups all show distinct positional and translational order of constituent unit. On the other hand, liquid crystals are positionaly and transitionally disordered (nematics) or transitionally ordered (smectics), but are characterized by orientational order of their constituent units. We therefore define their state by their molecular orientation, which in turn results in the concept of orientational order.

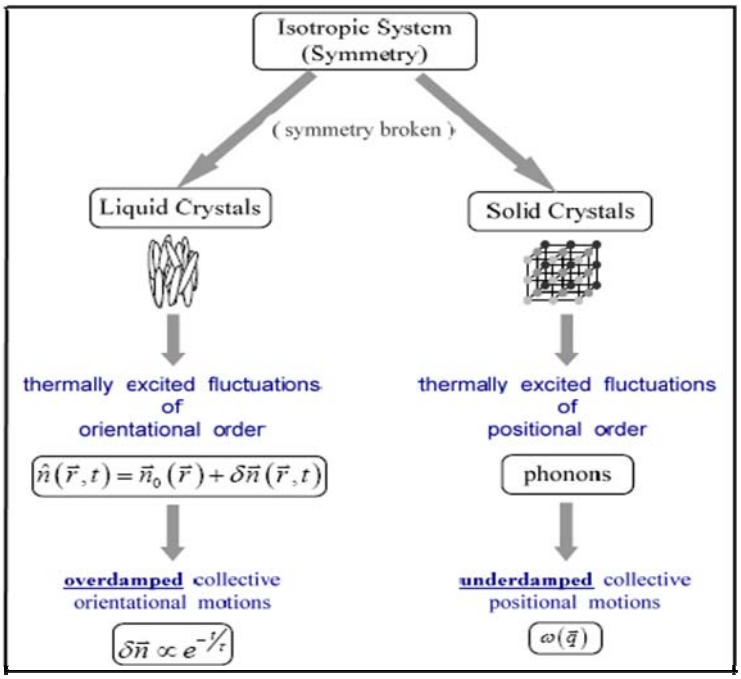

Fig. 1-3-3 The comparison of positional order in solids crystals and orientational order in nematic liquid crystals [2].

One extremely useful concept in describing a given state of matter is the collective excitations. This term relates to motions in a matter, where a large number of constituents participate coherently and cooperatively. For example, in solid crystals these collective excitations are phonons. They represent oscillations of a crystal lattice as a whole. Each constituent of the lattice cooperates in this collective motion coherently with its neighbors, which implies also the same frequency of oscillation of all atoms in a crystal for a given phonon mode. The analogy to the phonons in solid crystals is the orientational fluctuations in liquid crystals. Although liquid crystals are generally positionally disordered, the orientation of the molecules fluctuates coherently over extremely large distances. We have therefore time and space coherent motion of the director of liquid crystal. In particular, the collective excitations are usually underdamped and oscillatory in solid crystals while the collective modes in liquid crystals are always overdamped. This indicates that in liquid crystals the inertial forces are much smaller that the viscous forces, that originate from the positional disorder of these phases [4]. The above concepts are of great importance for they are the basis of this thesis.

1.3.2 The Physics of Surface-Stabilized Ferroelectric Liquid Crystal

As mentioned, ferroelectric liquid crystals are in chiral smectic-C phase. They show a translational order as well as orientational order. In the smectic-C phase, the periodic spacing of the mesogens along one axis, here we use the z axis, causes these molecules to form layers in the x-y plane as seen in Fig. 1-3-4. The director of each planar layer is tilted at an angle θ from the normal. This angle is temperature dependent and decreases with increasing temperature to become zero at a smectic-C to smectic-A phase transition. When the molecule is chiral, successive smectic-C layers show a gradual change in the direction of tilt, such that the director precesses about the z axis from layer to layer, always lying on the surface of a hypothetical cone of angle 2θ as illustrated in the Fig. 1-3-4. The angle around the circle of precession is known as the azimuthal angle φ, which therefore creates a helical structure in the chiral smectic C (SmC*) phase with the pitch being the distance along the z axis needed to reach the same molecular orientation. In addition to producing this helical structure, chirality also results in a spontaneous polarization, shown by the blue arrow in Fig. 1-3-4. This polarization vector is perpendicular to the molecule and contained in the layer plane. Therefore, a bulk SmC* sample, free to develop its helical structure,

will not show ferroelectric behavior since the spontaneous polarization will average to zero over one pitch.

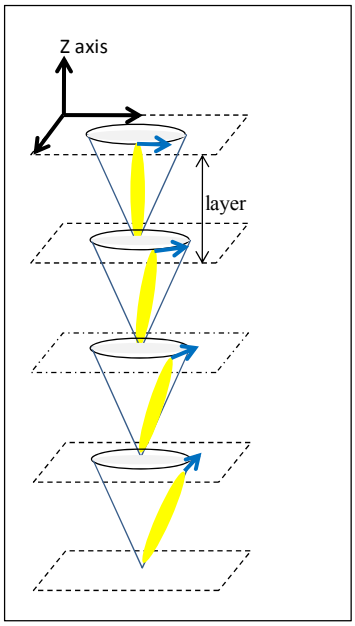

Fig. 1-3-4 The configuration of a helical structure in the chiral smectic-C* phase. The angle between the long axis of molecules and the layer normal are the same from layer to layer. The blue arrow represents its spontaneous polarization

The first ferroelectric liquid crystal molecule was synthesized with a structure similar to molecules that forms the smectic-C* liquid crystal phase. Nevertheless, the spontaneous polarization that a ferroelectric material should possess can be made up with an asymmetric carbon atom existing near one end of the molecule. This carbon atom is bound to four different atoms, thus it breaks inversion symmetry that a smectic–C* phase originally possesses. The broken inversion symmetry is how the chiral part of the whole molecule comes from. The temperature range corresponding

to different phases and the structure formula of this ferroelectric liquid crystal are shown below.

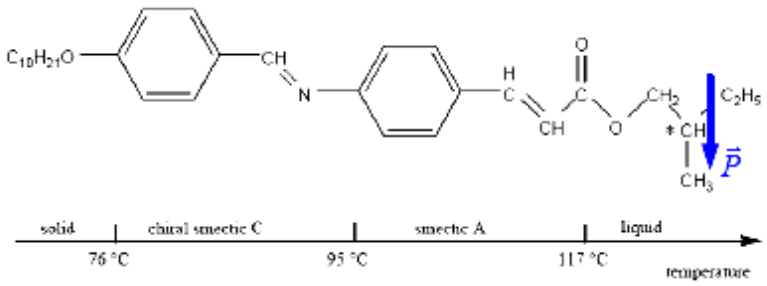

Fig. 1-3-6 The first ferroelectric liquid crystal molecule DOBAMBC. The carbon atom marked by an asterisk (*) is referred to as an asymmetric one. $\vec{P}$ represents the spontaneous polarization of the molecule [3].

At the year 1980, Clark and Lagerwall proposed a way to suppress the helix and developed the surface stabilized ferroelectric liquid crystal (SSFLC) arrangement shown in Fig. 1-3-5. The helix is constrained by using a cell gap that is less than the helical pitch. Interaction forces between the liquid crystal and the bounding plates unwind the intrinsic helix. Symmetry arguments show that this boundary condition also causes the molecular orientation for each layer to be the same and the material exhibits ferroelectric behavior. The director is favored to lie in the plane of the bounding plates. Because of this condition and the fact that the director is constrained to be at a certain angle from the normal to the layer, there are two stable states. The polarization vector, therefore, must be normal to the bounding plates and its two states

are in opposite directions. These two states are shown in the diagram Fig. 1-3-5. The up state is shown by the yellow molecule, while the down state is shown by the dotted line. Note how both states lie along the cone and are in the plane of the bounding plate.

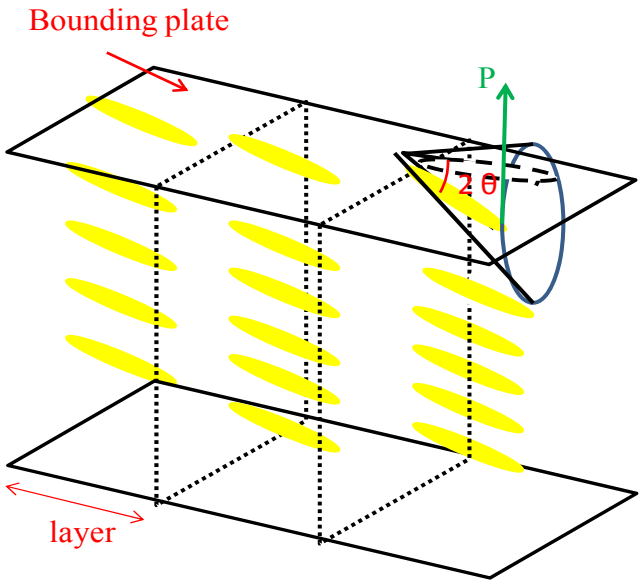

Fig. 1-3-5 two bistable states of a bookshelf type surface-stabilized ferroelectric liquid crystal device. When applying external electric field on the bounding plates, the spontaneous polarization would couple to the electric field and switches the state.

1.3.3 The electro-optic property of SSFLC

Liquid crystal electro-optic effects are important because they do not require the emission of light; instead they modify the passage of light through the liquid crystal

either by light scattering, modulation of optical density, or color changes. The salient properties are low-voltage operation, very low power dissipation, size and format flexibility, and washout immunity in high-brightness ambience.

As with all liquid crystals, the electro-optic effects in ferroelectric liquid crystals are obtained by manipulation of the molecular orientation, given by $\vec{n}$, with an electric field. In this case, with a macroscopic polarization in the medium, a number of new and interesting electro-optic effects are possible. First of all, the medium will normally couple much more strongly to an applied electric field than nonferroelectric liquid crystals. The ferroelectric torque density is of the order $P_S E$ and will, at least up to reasonable fields, be larger than the dielectric torque density of the order $\Delta\varepsilon_0 E^2$. But the more interesting thing is that we have to deal with a linear effect, which means that the torque applied to the local polarization vector is sensitive to the direction of the field, so that the polarization orientation will be able to follow sign reversals. This means that, in contrast to the nematic case, one is able to switch both ON and OFF in time much shorter that the viscous relaxation time of the material. The first observation of a linear electro-optic effect in the bulk chiral smectic-C* was reported by R. B. Meyer and co-workers in their article on the discovery of ferroelectricity in liquid crystals in 1975. Although the reported effect seemed not to be of practical interest, it was N. A. Clark and S. T. Lagerwall who noticed the technological

importance of a large electro-optic effect, when a ferroelectric smectic-C* phase is constrained in a thin layer between two glass plates.

The principle of the operation of the so-called “Surface Stabilized Ferroelectric Liquid Crystal (SSFLC)” is shown in Fig. 4-1-1. When a bulk helical ferroelectric smectic-C* is constrained between the closely spaced glass plates to form the bookshelf geometry, the interaction forces between the liquid crystals molecules and the surface plates are transmitted through the structure by elastic stress and result in an unwinding of the smectic-C* helix. This unwinding structure takes place if the plates are spaced close enough. Thus we get a homogeneously polarized ferroelectric state which can be switched by an external electric field. The ferroelectric liquid crystal is therefore a dielectric in a transparent capacitor. Voltages that are applied across the capacitor plates produce linear electro-optical switching of the polarization. We therefore get two distinct unwound states of uniform molecular orientation with opposite signs of the spontaneous polarization pointing either **left** (i.e., +θ) or **right** (i.e., -θ).

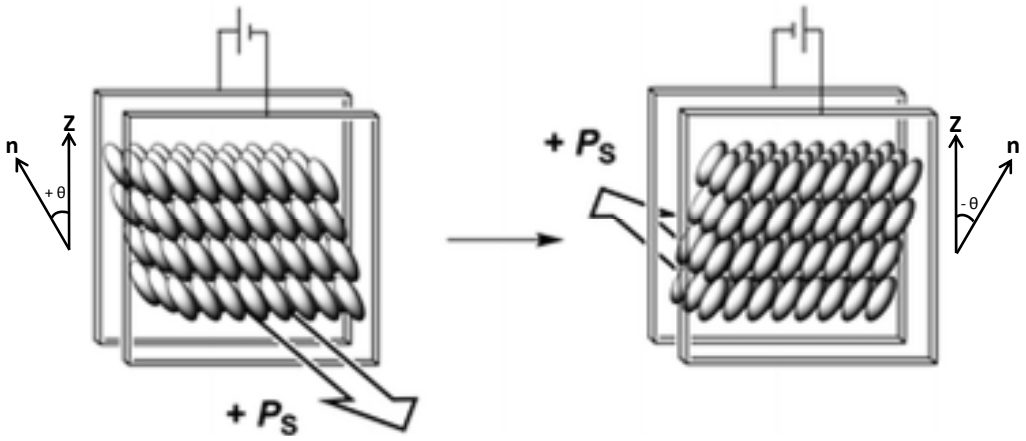

Fig. 1-3-6 The principle of operation of the SSFLC, invented by N. A. Clark and S. T. Lagerwall. The vectors z (layer normal) and n (molecular director) are in the plane of the page and form a tilt angle θ; Ps denotes the macroscopic spontaneous polarization.

For the state with the polarization pointing **outward**, the director field points in the " left " direction with respect to the smectic-C* layer normal. On the other hand, for the inwards polarization, the director points in the "right" direction, making an angle of 2θ with respect to the left direction. Let us remind that the optical properties of ferroelectric liquid crystals are determined by the director field $\vec{n}$ and the principal optic axis which is parallel to this director. The optical axis therefore changes its orientation by twice the tilt angle θ, when the direction of the spontaneous polarization is reversed by the external electric field. The tilt angle is of the order of 27.5 deg, which means that the direction of the optical axis in SSFLC switches for ≒ 55.1 deg when an alternating voltage is applied across the SSFLC cell. This switching can be easily observed between crossed polarizers. If these polarizers are oriented so

that the input polarization is along one of the extreme direction of the director, a switching between a “ dark ” and a “ bright” state is observed. In the “dark” state, the optical axis of the structure is aligned along the direction of the input polarizer, whereas in the “ bright ” state, it makes a double tilt angle with respect to the input polarizer. Due to birefringence of a liquid crystal, the ordinary and extraordinary waves travel with different speeds though the cell and interfere at the output. For a proper thickness, the phase difference will result in an elliptically polarized output light, which would transmit through the back polarizer. The SSFLC therefore represents a birefringent plate, where the direction of the optical axis can be switched over large angles with relatively small electric fields.

1.3.4 The Optical Properties of Surface-Stabilized Ferroelectric Liquid Crystal

In the ferroelectric smectic-C* phase, each smectic layer can be considered as a weakly biaxial smectic-C* phase, which could be described by dielectric tensor $\underline{\varepsilon}$ with the eigenvalues $\varepsilon_1, \varepsilon_2$ and ε_3

$$\underline{\varepsilon} = \begin{bmatrix} \varepsilon_1 & 0 & 0 \\ 0 & \varepsilon_2 & 0 \\ 0 & 0 & \varepsilon_3 \end{bmatrix} \tag{1.1}$$

However, the difference between ε_1 and ε_2 is usually small (*i.e.*, their physical properties in the two mutually orthogonal directions perpendicular to the director are physically equivalent), so that each layer of the smectic-C* can be considered as an optically uniaxial layer, with the optical axis, $\vec{k}$, tilted at a tilt angle θ with respect to the helical axis and the azimuthal angle φ defined as the angle between x axis and the in-plane projection of molecular tilt $\vec{\xi}$, as shown in Fig. 1-3-7. As a result, the optical properties of ferroelectric liquid crystal with unwinding helix (*i.e.*, also called surface-stabilized ferroelectric liquid crystal) can be regarded as those of nematic liquid crystals. In word, surface-stabilized ferroelectric liquid crystal is an optical uniaxial medium with birefringence characterized by two principal refractive indices. The refractive index, which is given by $n = \frac{c}{\upsilon}$, is inverse proportional to the velocity of light υ in the medium, where c denotes the speed of light in vacuum.

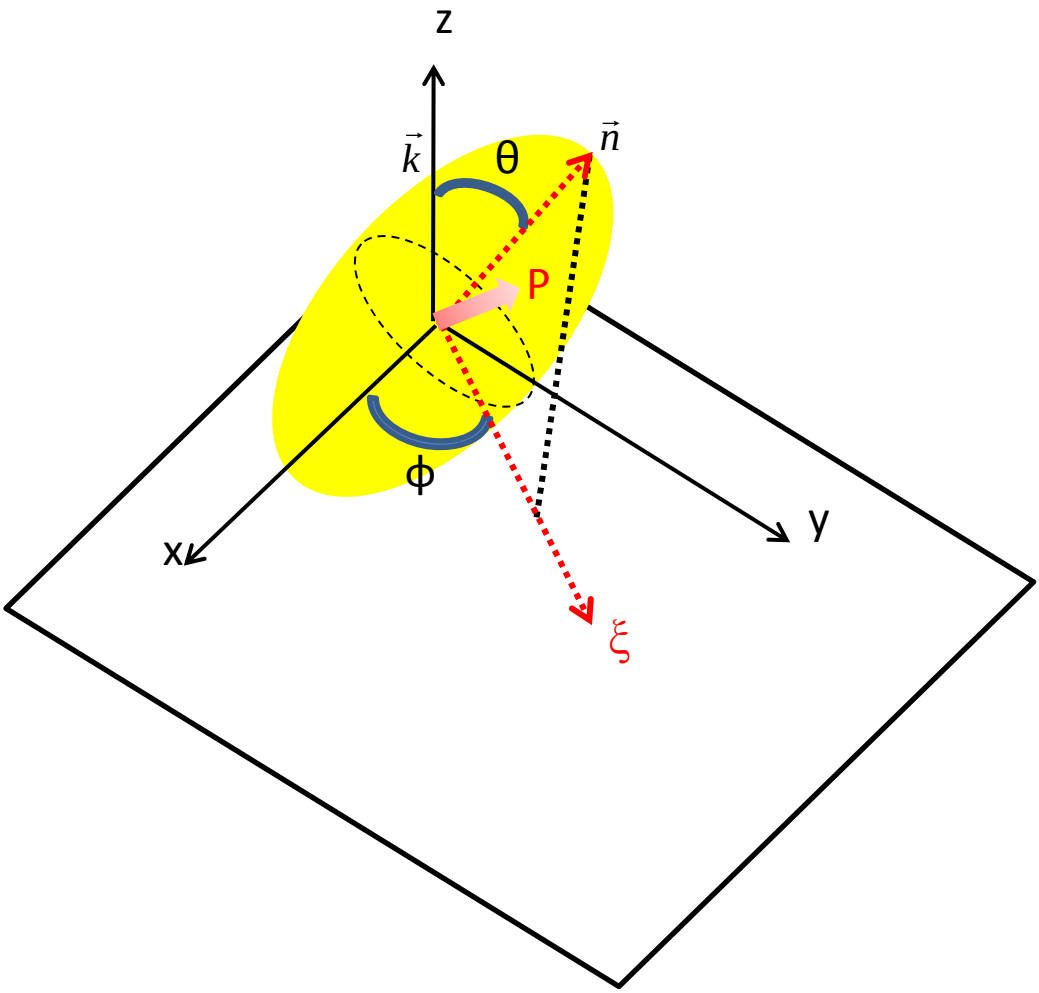

Fig. 1-3-7 The local orientation of the dielectric tensor in the smectic-C* phase. The spontaneous polarization, $\vec{P}$, is in the direction of $\vec{k} \times \vec{\xi}$ by definition. $\vec{n}$ and $\vec{\xi}$ denote the long axis of ferroelectric liquid crystal molecule and the in-plane projection of molecular tilt, respectively.

Accordingly, we could express the director $\vec{n}$ of ferroelectric liquid crystals in bookshelf geometry, the in-plane projection of $\vec{n}$ director, $\vec{\xi}$, the spontaneous polarization $\vec{P}$ and the layer normal $\vec{k}$ in the xyz-coordinate system as follows:

$$\begin{cases} \vec{n} = (\sin\theta\cos\phi, \sin\theta\sin\phi, \cos\theta), \\ \vec{k} = (0,0,1) \\ \vec{\xi} = (\cos\phi, \sin\phi, 0), \\ \vec{P} = (-\sin\phi, \cos\phi, 0), \end{cases} \tag{1.2}$$

where θ is the molecular tilt angle, and φ is the azimuthal angle of the ξ-director measured from the x-axis.

When a polarized optical beam impinges on nematic liquid crystals with rod-like shape, it would experience two distinct indices of refraction. The propagation of light along the optic axis would be independent of its polarization; its electric field is everywhere perpendicular to the optic axis and it is called the ordinary- or o-wave. The light wave with electric field parallel to the optic axis is called the extraordinary- or e-wave. An illustration of refractive index ellipsoid, which describes the dielectric properties of a material when they are measured in all directions, is shown below. The z axis in this figure is considered the optic axis in this model. A cross section is drawn through the ellipse, which yields the refractive index ellipse for waves traveling normal to that section. The major and minor axes of the ellipse denote the refractive indices encountered by the slow and fast waves.

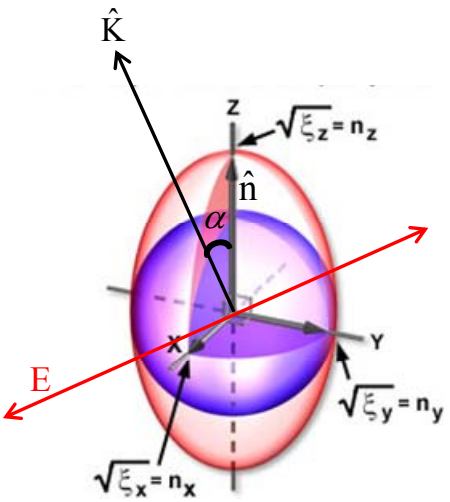

$$\frac{n_{eff}^{\ 2}\sin^2\alpha}{n_{//}^{\ 2}} + \frac{n_{eff}^{\ 2}\cos^2\alpha}{n_{\perp}^{\ 2}} = 1$$

n_{eff} : The refractive index of e-wave.

$\hat{K}$: The direction of light propagation

Fig. 1-3-8 A diagrammatic illustration of refractive index ellipsoid. The radius of the ellipsoid yields the refractive index n_{eff}. A cross section through the center of the ellipsoid produces a refractive index ellipse denotes the refractive indices encountered by the slow and fast waves, which vibrate with their electric displacement vectors along those two axes.

1.4 The Fluctuation Correlation of the LC director in a surface-stabilized ferroelectric liquid crystal cell

In section 1.3, we have learned that liquid crystals are states between liquid and crystals. Matters in these states are fluid, flexible substrate with a small amount of order; thus they are extremely sensitive to weak external perturbations such as temperature, electric field and so on. That is to say, in response to external perturbations, the orientation of liquid crystal molecules fluctuates coherently over extremely large distances as we have discussed in previous sections. This remarkable

characteristic plus their optical properties make it possible to detect the dynamics of liquid crystals under external perturbations by light scattering.

In order to realize the essence of fluctuation correlation in the physical system of surface-stabilized ferroelectric liquid crystals, we must introduce the basic concept of dynamic light scattering first.

1.4.1 Introduction to Elastic Light Scattering

In an elastic light scattering experiment, a monochromatic beam of laser impinges on a sample and is scattered into a detector placed at an angle δ with respect to the transmitted beam. The intersection between the incident beam and the scattered beam defines a volume V, called the scattering volume or the illuminated volume. A schematic representation of the light scattering experiment is shown in Fig. 1-4-1.

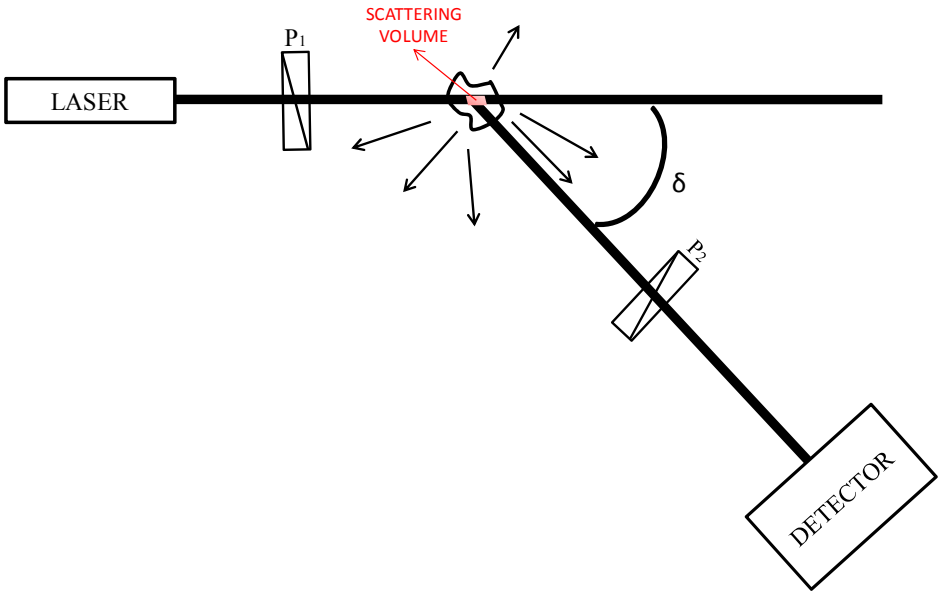

Fig. 1-4-1 An illustration of scattering volume and angleδin a light scattering experiment.

In an idealized light-scattering experiment, the incident light is a plane electro-magnetic wave. When the molecules in the illuminated volume are subjected to this incident electric field, their constituent charges experience a force and are thereby accelerated. According to classical electromagnetic theory, an accelerating charge radiates light. When visible light is incident upon the medium, the atoms in a subregion of the illuminated volume, small compare to the cube of the incident light wavelength, see essentially the same incident electric field. If many subregions of equal size are considered, the scattered electric field is the superposition of the scattered fields from each of them. If the subregions are optically identical, that is, each has the same dielectric constant, there will be no scattered light in other than the forward direction. This is so because the wavelets scattered from each subregion are

identical except for a phase factor that depends on the relative positions of the subregions. If we ignore surface effects, it is clear that for a large medium, each subregion can always be paired with another subregion whose scattered field is identical in amplitude but opposite in phase and will thus cancel, leaving no net scattered light in other that the forward direction. On the contrary, if the regions are optically different, that is, have different dielectric constants, then the amplitudes of the light scattered from the different subregions are no longer identical. Complete cancellation will no longer take place, and there will be scattered light in other that the forward direction. Thus in this semi-macroscopic view, originally introduced by **Einstein**, light scattering is a result of local fluctuations in the dielectric constant of the medium.

1.4.2 Orientational Fluctuations in Surface-Stabilized Ferroelectric Liquid Crystal Cells

Combining the above concepts that has been discussed, we have come to a conclusion: it is the fluctuations of the optical axes of molecules in surface-stabilized ferroelectric liquid crystal that leads to different dielectric constants in the illuminated volume and give rise to light scattering. In short, the dynamics of the molecules is thus revealed in the light scattering. Having attained the basic concept of dynamic

light scattering, we can now proceed with the relation between fluctuations and light scattering from surface-stabilized ferroelectric liquid crystal through a mathematical description.

Our experiment set up has already been discussed in section 1.2. Using Jones' calculus, one can describe an electric field that goes through the optical elements used in the experiment and is give by

$$\begin{bmatrix} \tilde{E}_x \\ \tilde{E}_y \\ \tilde{E}_z \end{bmatrix} = \begin{bmatrix} 0 & 0 & 0 \\ 0 & 1 & 0 \\ 0 & 0 & 0 \end{bmatrix} \cdot \begin{bmatrix} \cos\phi\sin\theta & \cos\phi\cos\theta & -\sin\phi \\ \sin\phi\sin\theta & \sin\phi\cos\theta & \cos\phi \\ \cos\theta & -\sin\theta & 0 \end{bmatrix} \cdot \begin{bmatrix} e^{in_{//}\kappa d} & 0 & 0 \\ 0 & e^{in_{\perp}\kappa d} & 0 \\ 0 & 0 & e^{in_{\perp}\kappa d} \end{bmatrix} \cdot$$
$$\begin{bmatrix} \cos\phi\sin\theta & \sin\phi\sin\theta & \cos\theta \\ \cos\phi\cos\theta & \sin\phi\cos\theta & -\sin\theta \\ -\sin\theta & \cos\phi & 0 \end{bmatrix} \cdot \begin{bmatrix} 0 \\ 0 \\ 1 \end{bmatrix} \cdot E_0$$
$$= \begin{bmatrix} iE_0 e^{i\bar{n}\kappa d} \sin 2\theta \cos\phi \sin\dfrac{\Delta n\kappa d}{2} \\ 0 \\ 0 \end{bmatrix}$$

$$\Delta n = n_{//} - n_{\perp}$$
$$k = \frac{2\pi}{\lambda_{air}} \tag{1.3}$$

Where E_0 and $\tilde{E}_i$ $(i = x, y, z)$ represent incoming and outgoing electric field, respectively, and d is the cell gap of SSFLC. The output light is detected by a photomultiplier tube to yield an intensity with the following form

$$\tilde{I} = I_0 \sin^2\frac{\Gamma}{2}\cos^2\phi$$
$$I_0 = {E_0}^2 \sin^2 2\theta \tag{1.4}$$

.

Where $\Gamma = \frac{\Delta n \kappa d}{2}$ represent the phase retardation. Eqn. (1.4) reveals that the fluctuation of φ angle can affect the intensity of scattered light.

Chapter 2

Introduction to Stochastic Process in Liquid Crystal

2.1 Introduction

The thermally excited dynamics in SSFLC is a complex process which is closely related to the microscopic theory. To begin with, we must introduce a simple and well known example of the thermal molecular motions- the Brownian motion. Observing colloidal particles floating in a liquid medium under an ultramicroscope, one would find the irregular motion of colloidal particles. Such a random behavior has been proved to be direct evidence of thermal molecular motion. To be more specific, the impacts exerted by the liquid molecules can be considered as a random force that drives the particles to act irregularly. This is a classical example of thermal molecular motion which always exists, even in thermal equilibrium, as a fluctuation. Similar to the motions of colloidal particles in a liquid (i.e., the Brownian motion), the thermal energy also excites ferroelectric liquid crystal molecules and induces collective excitation which, however, is quite different from the Brownian motion because of the structure of matter. Here, the term “collective excitation” means a large number of FLC molecules fluctuate coherently and cooperatively as introduced in chapter one.

From the point of view, it is reasonable to assume that inside the SSFLC cell, the FLC molecules would aggregate into groups, and each group fluctuates as a whole and collides with one another. The constant collisions coming from all direction act as a random driving force on the FLC molecular group to maintain the incessant irregular motion. With the random force in the system, the dynamics of SSFLC could no longer be exact determined by a given physical condition but it becomes a stochastic process.

2.2 Stochastic Process

In probability theory, a random variable is the counterpart to a deterministic variable. A random variable does not possess a deterministic value. A physical process with controlling parameters being random variables is called a "stochastic process" as illustrated in **Fig. 2-1-1**. Instead of dealing with an exact outcome of how the process might evolve under time, in a stochastic process there is some indeterminacy in its future evolution described by probability distributions.

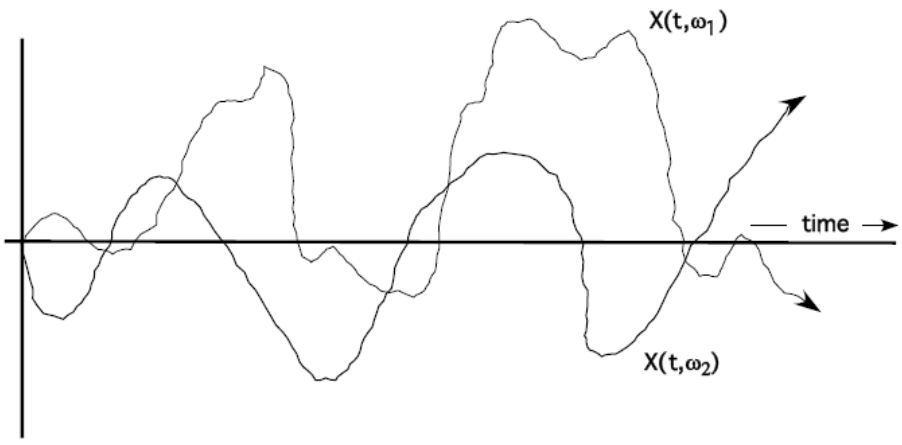

Fig. 2-2-1 Two sample paths of a stochastic process $X(t, \omega)$ with a controlling parameter ω being random variable.

Let us consider a property ***A*** that depends on the positions and momenta of all the particles in the system. By virtue of their thermal motions the particles are constantly jostling around so that their positions and momenta are changing in time, and so too is the property ***A***. Although the constituent particles are moving according to Newton's equation, their very value makes their motions and property ***A*** appears to be somewhat random. This physical process with property ***A*** is a generalized example of stochastic process for granular matter.

Stochastic processes of a particular type, **Markov** processes, play an important role in natural phenomena. The **Markov** process does not depend on any of its earlier values explicitly to advance itself from time t to time $t + dt$. In other words, knowledge of the present state of systems described by these processes determines the distribution of future states. In theory of statistics, a continuous **Markov** process guarantees that the increment $X(t+dt) - X(t)$ must have the analytical form of $\mathrm{A}(\mathrm{X}(t), t)dt + \sqrt{\mathrm{D}(\mathrm{X}(t), t)}\, N(t)\sqrt{dt}$. Here $\mathrm{A}(\mathrm{X}(t), t)dt$ and $\mathrm{D}(\mathrm{X}(t), t)$ can be any smooth function with $\mathrm{D}(\mathrm{X}(t), t)$ non-negative, $N(t)$ denotes an uncorrelated unit normal random variable, that is, $N(t)$ is a random variable with its mean value equal to 0 and variance equal to 1. $N(t)$ is statistically independent of $N(t')$ when $t' \neq t$ '.

From the above, we obtain

$$\mathrm{X}(t+dt) = \mathrm{X}(t) + \mathrm{A}(\mathrm{X}(t), t)dt + \sqrt{\mathrm{D}(\mathrm{X}(t), t)}\ N(t)\sqrt{dt}. \tag{2.1.1}$$

Rearranging Eq. (2.1.1) yields the differential form

$$\frac{\mathrm{X(t+dt) - X(t)}}{dt} = \mathrm{A(X(t), t)dt} + \frac{\sqrt{\mathrm{D(X(t), t)}}N(t)}{\sqrt{dt}}. \tag{2.1.2}$$

For Eq. (2.1.2) with

$$\begin{aligned} \mathrm{A(X(t), t)} &= -\frac{1}{\tau}\mathrm{X(t)} \\ \mathrm{D(X(t), t)} &= \mathrm{c}, \end{aligned} \tag{2.1.3}$$

is called an **Ornstein-Unlenbeck** process with relaxation time τ and diffusion constant c. Thus, we can transform eqs. (2.1.1) into

$$\frac{\mathrm{dX(t)}}{dt} = -\frac{1}{\tau}\mathrm{X(t)dt} + \sqrt{\mathrm{c}}\Gamma(t), \tag{2.1.4}$$

where the Gaussian white noise process $\Gamma(t)$ was defined as $\Gamma(t) \equiv \lim_{dt\to 0} N(0, \frac{1}{dt})$.

To solve such an equation of (2.1.4), one needs to draw support from the statistical mathematics [4] and derives

$$\mathrm{X(t)} = \mathrm{N}\left(x_0 e^{-t/\tau}, \frac{c\tau}{2}(1 - e^{-2t/\tau}) \right). \tag{2.1.5}$$

with $x_0 e^{-t/\tau}$ and $\frac{c\tau}{2}(1 - e^{-2t/\tau})$ being the mean and variance of X(t), respectively. Moreover, we would need to derive the variance of $\frac{\mathrm{dX(t)}}{\mathrm{dt}}$ for the following sections. First, we start with

$$< (\frac{dX(t)}{dt})^2 >= \frac{d}{dt} < X(t)\frac{dX(t)}{dt} > - < X(t)\frac{d^2X(t)}{dt^2} > \quad . \tag{2.1.6}$$

Since the operations of taking a time derivative and taking an ensemble average

commute, eqn. (2.1.6) is then valid [5]. From eqn. (2.1.6), we realize that we need to solve $< X(t)\frac{d^2X(t)}{dt^2} >$ and $< X(t)\frac{dX(t)}{dt} >$ in advance.

Let us take a time derivative to eqn. (2.1.4) and multiply X(t) on both sides. After taking an ensemble average we then have

$$< \mathrm{X(t)}\frac{\mathrm{d^2X(t)}}{dt^2} > + \frac{1}{\tau} < X(t)\frac{\mathrm{dX(t)}}{\mathrm{dt}} >= \sqrt{c} < X(t) >< \frac{d}{dt}\Gamma(t) > \quad . \tag{2.1.7}$$

Note that $\sqrt{c} < X(t)\frac{d\Gamma(t)}{dt} >= \sqrt{c} < \mathrm{X(t)} >< \frac{d\Gamma(t)}{dt} >$ because of the statistical independency of X(t) and $\Gamma(t)$, and it vanishes for $\lim_{dt\to 0}\Gamma(t) = N(0,\frac{1}{dt})$. Hence eqn. (2.1.6) can be reduced to

$$< (\frac{\mathrm{dX(t)}}{dt})^2 >= \frac{d}{dt} < X(t)\frac{\mathrm{dX(t)}}{\mathrm{dt}} > + \frac{1}{\tau} < X(t)\frac{\mathrm{dX(t)}}{\mathrm{dt}} > . \tag{2.1.8}$$

Again, we multiply X(t) on both side of eqn. (2.1.4) and get

$$< \mathrm{X(t)}\frac{\mathrm{dX(t)}}{\mathrm{dt}} > + \frac{1}{\tau} < X^2(t) >= \sqrt{c} < \Gamma(t)X(t) >= 0 \quad . \tag{2.1.9}$$

With the help of eqn. (2.1.5) we obtain

$$< \mathrm{X(t)}\frac{\mathrm{dX(t)}}{\mathrm{dt}} >= -\frac{1}{\tau} < X^2(t) >= -\frac{1}{\tau}[\frac{\mathrm{c}\,\tau}{2}(1\text{-}e^{-2t/\tau}) + x_0^{\,2}e^{-2t/\tau}] . \tag{2.1.10}$$

Finally, by substituting eqn. (2.1.10) into eqn. (2.1.8) we arrive

$$\lim_{t\to\infty} Var\{\frac{\mathrm{dX(t)}}{\mathrm{dt}}\} = \frac{c}{2\tau}, \tag{2.1.6}$$

which is useful in a later chapter.

.

2.2.1 Introduction to Stochastic Differential Equation

The **Markov** process is a mathematical model for a system with random

evolution in time, and thus it is defined as a stochastic differential equation. A **stochastic differential equation (SDE)** is a differential equation in which one or more of the terms are random variables. Through the equation, the time behavior of a physical property that shows fluctuations could be fully described in terms of probability [6]. To date, the stochastic differential equation (SDE) models play a relevant role in many application areas including biology, epidemiology and population dynamics, mostly because they can provide an additional degree of realism if compared to their deterministic counterparts.

A well-known SDE example that has successfully described Brownian motion is the **Langevin** equation, which states the relation between spontaneous fluctuation and the energy dissipation. This idea is the spirit of the granular nature of matter which also stands in the system of SSFLC but probably with a different form. To derive the specific relation in SSFLC, let us begin a brief discussion about Brownian motion of colloidal particles suspending in a liquid medium.

2.2.2 Derivation of the Fluctuation-Dissipation Theorem (FDT) of Brownian Motion

Consider a particle of mass m immersed in a liquid medium at temperature T, and

the corresponding velocity v. The particle's dynamic behavior governed by **Newton**'s second law of motion is

$$m\frac{d\vec{v}}{dt} = -\gamma\vec{v} + \vec{F} \tag{2.2.1}$$

where γ is a positive constant called "friction constant" which is proportional to the viscosity of the liquid according to Stokes' law, and $\vec{F}$ denotes the random force generated from random bombardment by the molecules. Accordingly, $\vec{F}$ is a white noise process with zero mean value and does not depend on any of its earlier values explicitly to advance itself from time t to time t + dt. In short, eqn. (2.2.1) can be considered as a **Morkov** process and the solution has already been given from section 2.1 [7]

$$v(t) = N\left(v_0 e^{-t/\tau}, \frac{c\tau}{2}(1 - e^{-2t/\tau})\right), \tag{2.2.2}$$

Here we define the magnitude of $\vec{F}$ as $m\sqrt{c}$ and relaxation time $\tau = m/\gamma$ for simplicity.

According to equipartition theorem, the energy associated with fluctuations in each degree of freedom is $\frac{k_B T}{2}$, that is,

$$\frac{1}{2}mVar\{v(t \to \infty)\} = \frac{cm\tau}{4} = \frac{k_B T}{2}, \tag{2.2.3}$$

Combining Einstein's relation $< x^2(t) >= 2Dt,$ where D is defined as diffusion constant, we have come to

$$D = \frac{k_B T}{\gamma}, \tag{2.2.4}$$

The equation makes physical sense perfectly as we could imagine that particles diffuse faster in a higher surrounding temperature as well as in a less viscous liquid medium. By some further substitution we could obtain the fluctuation-dissipation theorem as follows

$$c = \frac{6k_B T\gamma}{m^2}, \tag{2.2.5}$$

Eqn. (2.2.5) illustrates that whenever a physical system shows fluctuating dynamics in some property, there exist an energy dissipation channel accompanying that physical property. In the case of Brownian motion, the thermally induced random impacts of surrounding molecules generally cause two kinds of effect: firstly, they act as a random driving force on the Brownian particles, secondly, they give rise to the frictional force γ for a forced motion [8]. This in turn means that the frictional force and the random force must be related, because both come from the same origin- the random bombardment. In a way, fluctuation and dissipation are like two sides of one coin.

2.2.3 Stochastic Process in the Physical system of Surface-Stabilized Ferroelectric Liquid Crystal

To successfully construct an SDE model of surface-stabilized ferroelectric liquid

crystal, we begin with the free energy of liquid crystal. The thermodynamical potential per unit volume ***E***, whose minima define the stable states of the system, can be written as [9, 10]

$$\mathrm{E}_{free} = e_{elastic} + e_{dielectric} + e_{couple} \tag{2.2.6}$$

Let us first consider the elastic free energy which varies with deformations that a physical system suffers. When liquid crystals deform with external field, three types of deformation energy would occur. They are splay, twist and bend as sketched in Fig. 2-2-1. Hence the elastic free energy density of the deformed liquid crystals can be expressed in terms of the three deformations and is given by [10]

$$\hat{e}_{elastic} = \frac{1}{2}K_1(\nabla \cdot \hat{n})^2 + \frac{1}{2}K_2(\hat{n} \cdot \nabla \times \hat{n})^2 + \frac{1}{2}K_3(\hat{n} \times \nabla \times \hat{n})^2, \tag{2.2.7}$$

where $K_i (i = 1,2,3)$ introduced in eqn (2.2.6) are **Frank** elastic constants, and they are respectively associated with the three types of deformation displayed in Fig. 2-2-1.

K_1: conformations with div $n \neq 0$ (splay);

K_2: conformations with $n \bullet$ curl $n \neq 0$ (twist);

K_3: conformations with $n \times$ curl $n \neq 0$ (bend).

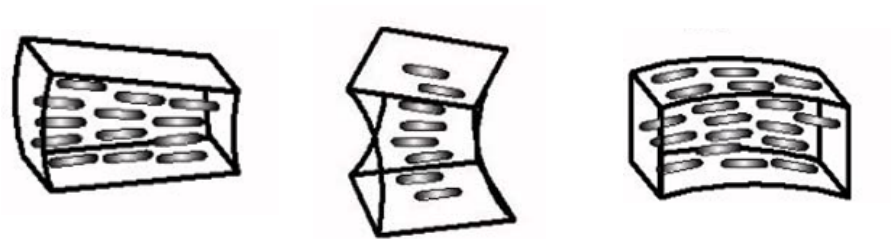

splay $\nabla \cdot \hat{n} \neq 0$ twist $\hat{n} \cdot \nabla \times \hat{n} \neq 0$ bend $\hat{n} \times \nabla \times \hat{n} \neq 0$

Fig. 2-2-1 The three types of deformation commonly occurring in liquid crystal.

However, the elastic free energy of a chiral smectic C liquid crystal would be better to start with the $\vec{\xi}$ director. If the layer structure does not change, the elastic free energy density $e_{elastic}$ is given by [11]

$$\hat{e}_{elastic} = \frac{1}{2}B_1\{\vec{k}\cdot(\nabla\times\vec{\xi})\}^2 + \frac{1}{2}B_2(\nabla\cdot\vec{\xi})^2 + \frac{1}{2}B_3\{\vec{\xi}\cdot(\nabla\times\vec{\xi})\}^2$$
$$- B_{13}\{\vec{k}\cdot(\nabla\times\vec{\xi})\}\{\vec{\xi}\cdot(\nabla\times\vec{\xi})\} \qquad (2.2.8)$$

Where the smectic elastic constants B_1, B_2, B_3, B_{13} are relevant to the pure bend, splay, twist respectively of the tilt director $\vec{\xi}$. In fact, pure distortion of $\vec{\xi}$ can imply mixed distortions of the director $\vec{n}$: for example both B_1 and B_3 comprise mixed symmetrical twist-bend deformations of $\vec{n}$, whereas B_2 implies only $\vec{n}$-splay distortion. The new elastic constants read [12]:

$$\begin{aligned} B_1 &= \sin^2\theta[K_2\cos^2\theta + K_3\sin^2\theta], \\ B_2 &= K_1\sin^2\theta, \\ B_3 &= \sin^2\theta[K_2\cos^2\theta + K_3\sin^2\theta], \\ B_{13} &= \frac{1}{2}(K_3 - K_2)\sin^2\theta\sin 2\theta. \end{aligned} \qquad (2.2.9)$$

We could now derive the elastic free energy density of surface-stabilized ferroelectric

liquid crystals with bookshelf geometry by substitution of eqn. (1.2) into eqn. (2.2.7) and get

$$\hat{e}_{elastic} = \frac{1}{2}B_1\{\vec{k}\cdot(\nabla\times\vec{\xi})\}^2 + \frac{1}{2}B_2(\nabla\cdot\vec{\xi})^2 + \frac{1}{2}B_3\{\vec{\xi}\cdot(\nabla\times\vec{\xi})\}^2$$
$$= \frac{1}{2}(B_1\sin^2\phi + B_2\cos^2\phi)(\frac{\partial\phi}{\partial y})^2 \qquad (2.2.10)$$

With the help of one constant approximation suggested by ***de Gennes*** [10], eqn. (2.2.10) would deduce to the following given form

$$e_{elastic} = \int_0^d \hat{e}_{elastic}\,dy = \int_0^d \frac{1}{2}K_1\sin^2\phi(\frac{\partial\phi}{\partial y})^2\,dy \qquad (2.2.11)$$

The second term on the right hand side of eqn. (2.2.6) is the energy density $e_{dielectric}$ coupling to an electric field applied along the y-axis and is given by

$$e_{dielctic} = -\frac{1}{2}\vec{D}\cdot\vec{E} = -\frac{1}{2}\varepsilon_y E^2 \quad , \qquad (2.2.12)$$

where $\vec{D}$ is the electric displacement governed by Maxwell's equations of $\nabla\cdot\vec{D} = 0$. Finally, the third term e_{couple} referring to the coupling energy between spontaneous polarization P_s and the external electric field is given by

$$e_{couple} = -\vec{P}_s\cdot\vec{E} = -P_s E\cos\phi. \qquad (2.2.13)$$

The total energy per unit area of the cell can then be expressed as

$$E_{free} = e_{elastic} + e_{dielectric} + e_{couple} \qquad (2.2.14)$$

Introducing the rotational viscosity coefficient η, the equation of motion can be written in the form of a simple harmonic oscillator driven by thermal force $F_{thermal}$ and is given by [13]

$$\rho \frac{\partial^2 \phi}{\partial t^2} + \eta \frac{\partial \phi}{\partial t} = \frac{\delta E_{free}}{\delta \phi} + F_{thermal} \cdot \tag{2.2.15}$$

Where ρ denotes the material constant having the dimensions of moment of inertia per unit volume, and η represents the rotational viscosity of FLC. The unit of eqn. (2.2.15) is Newton · m^{-2}. Eqn. (2.2.15) tells us that the stable state is defined by the minima of the free energy E_{free} but perturbed by thermally induced random force. However, with the fact that the inertial forces in liquid crystals are much smaller than the viscous forces as indicated in section 1.3.1, eqn. (2.2.15) could be reduce to a simpler form as follows

$$\eta \frac{\partial \phi}{\partial t} = \frac{\delta E_{free}}{\delta \phi} + F_{thermal} \cdot \tag{2.2.16}$$

The equation above is also known as Landau-Khalatonilov equation. To solve eqn. (2.2.16), we must use Eular-Lagrange equation to find the minima of the free energy. That is, for any function ***J*** that can be expressed in the following form

$$J = \int_{x_1}^{x_2} f(\alpha, \alpha_x, x) dx \tag{2.2.17}$$

Its minima can be determined through the equation

$$\frac{\partial f}{\partial \alpha} = \frac{\partial}{\partial x} \frac{\partial f}{\partial \alpha_x} = 0 \quad . \tag{2.2.18}$$

Thus, the equation of motion in absence of external electric field becomes

$$\eta \frac{\partial \phi}{\partial t} = K \sin^2 \theta \frac{\partial^2 \phi}{\partial y^2} + F_{thermal} \cdot \tag{2.2.19}$$

To simplify eqn. (2.2.17) and focus on the ϕ angle fluctuations, we need to

extract ϕ variance of time dependence by separation of variables. On top of that, the boundary condition for function ϕ is given by

$$\begin{cases} \phi(0,t) = 0 \\ \phi(d,t) = 0 \end{cases}, \tag{2.2.20}$$

for the rubbing direction along the z axis as denoted in section 1.2. With the boundary condition shown above, we then use sine function to expand eqn. (2.2.19) and derive

$$\begin{aligned} &\phi(y,t) = \sum_{n=1}^{\infty} \psi(t) \sin \frac{n\pi y}{d}, \\ &\eta \frac{d\psi(t)}{dt} + \widetilde{K}\psi(t) = \frac{4}{\pi} F_{thermal}(t). \end{aligned} \tag{2.2.21}$$

Here $\Psi(t)$ is a time dependant function of ϕ and $\widetilde{K} = K \sin^2 \theta (\frac{\pi}{d})^2$. Moreover, $F_{thermal}$ can be expressed in terms of stochastic mathematics as

$$\frac{4}{\pi} \mathrm{F}_{\text{thermal}}(t) = \eta \sqrt{c} \Gamma(t) = \eta \sqrt{c} \lim_{dt \to 0} N(0, \frac{1}{dt}). \tag{2.2.22}$$

If we define $\frac{\eta}{\widetilde{K}} = \tau$, the solution of eqn. (2.2.20) becomes

$$\psi(t) = N\left(\phi_0 e^{-t/\tau}, \frac{c\tau}{2}(1 - e^{-2t/\tau}) \right). \tag{2.2.23}$$

As noted that the energy associated with fluctuations in each degree of freedom is $\frac{k_B T}{2}$, then

$$\frac{1}{2}\rho Var\{\omega(t \to \infty)\} + \frac{1}{2}\widetilde{K} Var\{\phi(t \to \infty)\} = \frac{1}{4}(\frac{c\rho}{\tau} + \widetilde{K}c\tau) = \frac{k_B T}{2}, \tag{2.2.24}$$

where ω is the angular velocity and has already been defined in section 2.1. We therefore obtain the fluctuation-dissipation theorem in the physical system of defect free SSFLC

$$c = \frac{2k_B T\tau}{\rho + \tilde{K}\tau^2}. \tag{2.2.25}$$

The above equation may look different from what we have deduced in Brownian motion, but it actually leads to the same result as eqn. (2.2.5). In our model, the random bombardment acts as a random force that pushes the FLC molecular group away from the stable state. At this point, the kinetic energy is partially dissipated though the random impact and the rest of the part would transfer to potential energy. When the FLC molecular recover itself to the stable state, it release its potential energy to kinetic energy, though which, the energy is again dissipated because of friction force caused by random impact. The only difference between eqn. (2.2.25) and eqn. (2.2.5) is just about energy transferring, but their relation between fluctuation and dissipation are basically the same. Both fluctuations are from the random bombardment which also results in friction force. The dynamics in the system of SSFLC must show some chaotic behavior due to the random impacts of FLC molecular groups. To deal with such a noise-like signal, the most efficient way is to analyze it through a correlation function.

2.3 Correlation Analysis

Time-dependent correlation functions have been used for a long time in the theory of noise and stochastic processes and have become very useful in many areas

of statistical physics and spectroscopy. Correlation function provides a concise method for expressing the degree to which two dynamical properties are correlated over a period of time. In this section we discuss some of the basic properties of these functions that are relevant to facilitate our understanding of light scattering spectroscopy.

To begin with, let us consider a physical property ***A*** that can be described by a stochastic differential equation. Generally, the property ***A*** exhibits a noise-like profile due to its random behavior and possesses the following features: the property ***A*** usually takes on different values at different positions in time axis, that is, $\mathrm{A}(t+\tau) \neq \mathrm{A}(t)$ in mathematics terms. However, when τ is small compared with the time scale characterizing the fluctuations in ***A***, ***A***(t+τ) would be very close to ***A***(t). As τ increases, ***A***(t+τ) and ***A***(t) are likely getting less and less similar. With the notion in mind, we could say that ***A***(t+τ) and ***A***(t) are correlated when τ is small, whereas ***A***(t) and ***A***(t+τ) are getting less and less correlated as τ gets larger. To specify this phenomenon more quantitatively, we need a measure of this correlation. An efficient and viable method is the autocorrelation function of the property ***A*** which is defined as

$$< \mathrm{A}(0)\mathrm{A}(\tau) >\equiv \lim_{T\to\infty}\frac{1}{T}\int_{0}^{T} A(t)A(t+\tau)dt. \qquad (2.3.1)$$

Here, a fact must be reminded that $< \mathrm{A}(0)\mathrm{A}(\tau) >=< A(t)A(t+\tau) >$ for

time-invariance. Second, with the principle of **Schwartz**'s inequality we derive [14],

$$< A(0)A(\tau) > \leq < \mathrm{A}(0)^2 > \qquad (2.3.2)$$

which implies that the delayed autocorrelation value (i.e., $\tau \neq 0$) will never exceed initial autocorrelation value (*i.e.*. $\tau=0$). To be more explicit, we can say that the autocorrelation function of a non-conserved, non-periodic property decays from its initial vale $<A^2>$ to $<A>^2$ in the course of time [14].

In light scattering experiments, photons impinging on the photon-detector produce amplified photon-electron current pulses as an input to the correlator electronics. Through which, the time-correlation function of the scattered field is computed in the discrete manner

$$< n(0)n(\tau) > \cong \lim_{N\to\infty} \frac{1}{N} \sum_{j=1}^{N} n_j n_{j+n} , \qquad (2.3.3)$$

where n_j is the number of photocounts during the time interval $j\triangle t$ to $(j+1)\triangle t$ and $\tau = n\triangle t$ with $\triangle t$ being the sampling time. Furthermore, the autocorrelation function of photon-counting fluctuations is related to the autocorrelation function of the short-time-averaged intensity fluctuations by the relationship

$$< n(t)n(t+\tau) >= \alpha^2 \Delta t^2 < \mathrm{I(t)I(t+}\tau) > . \qquad (2.3.4)$$

This relationship together with eqn. (1.4) allow us to get the correlation function of φ by simply measuring $<n(t)n(t+\tau)>$.

From the above context, we realize the necessity of the correlation analysis

applied in light scattering experiments. Now, we shall introduce its further improved technique, multiple tau autocorrelation, used in our experiments [15, 16]. Flex02-01D, which is made by Correlator.com, is a state-of-the-art commercial correlator. It has a quasi-logarithmic time scale, which is also why it is named “multiple tau”, where each channel has an individual sampling time (*i.e.*, the bin width) and delay time (*i.e.*, the delay from the measurement at time zero). With this quasi-logarithmic time-scale structure which will be described in Fig. 2.3.1, the sampling time increases with the delay time. This approach offers the advantage that a wide range of delay times can be measured with a limited number of correlation channels. For example, delay times between 0.2 μs and 50 ms can be obtained using only 128 channels. For the same range of delay times, a linear correlator would require 250,000 channels. In the presently used correlator which comprises 1152 channels, among which, channels 1-64 have a sampling time of 1.5625 ns. Each following group of 32 channels has an individual sampling time of twice that of the preceding group (*i.e.*, channels 65-96, 3.125 ns; channels 67-128, 6.25 ns; up to channels 1120-1152, 27s). Accordingly, there are 35 groups categorized by their bin width. The delay time of each channel is the accumulated sampling time of all preceding channels (channel 1, 0 ns; channel 2, 1.5625 ns; … ; channel 1152, 429.4963 s). Additional to each channel there is a delayed monitor M_{del} that accumulates all counts sampled in that channel. For every

group of channels with equal sampling time, there exists a direct monitor M_{dir} that accumulates all counts without delay time at a particular sampling time.

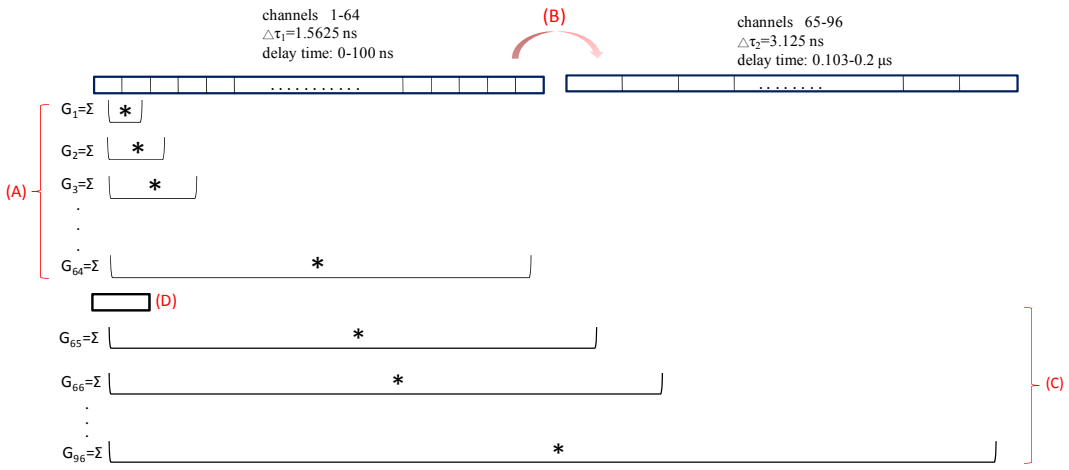

Fig. 2-3-1 Channel architecture of the digital correlator (A) The light intensity form the confocal volume is registered with a channel width of 1.5625 ns. After every measurement, three tasks are executed: (1) all channels are shifted to the right, channel (n - 1) to channel n, channel (n - 2) to channel (n – 1), … , channel 1 to channel 2. The new measurement is always stored in channel 1. (2) The products, that is depicted as *, of channel 1 and 2, of channel 1 and 3, etc., are calculated and added (i.e., Σ) to the correlation function $G(\Delta\tau_1)$, $G(2\Delta\tau_1)$, $G(3\Delta\tau_1)$, etc., respectively. The value of G(0) can be calculated by multiplying channel 1 with itself. (3) The delayed monitor is a register for every channel that sums up all counts that pass through a channel. Therefore, after each shift of channels the content of every channel is added to its delayed monitor. (B) Channels 63 and 64 are summed up and shifted to channel 65 which now acquires a width of 3.125ns. This happens at the end of every channel group. The last two channels with 3.125 ns (channel 95 and 96) are added to yield channel 97 with 6.25 width and so on. (C) Those channels that have a width of larger than 1.5625 ns (i.e., all channels after channel 64) are now correlated with a channel at 0 delay time of equal length. To achieve this, several channels can be summed up. Channels 1 + 2 act as the 0-delay-time channel for channels 65-96 (i.e., channel with 6.25ns width). The sum of channels 1-4 act as 0-delay-time channel for channels 97-128, and so on. Note that. For channels 1-64, the correlation is performed after every 1.5625 ns measurement, but, for channels with a width of 3.125 ns, the correlation will be done only every 3.125 ns, i.e.,

after 2 measurements of 1.5625 ns and so on. (D) The 0-delay-time channel with 3.125 ns width is shown. It is used for the correlations of channels with a width of 3.125 ns. The direct monitor is a register for every group of channels with equal length. In this register, the counts are stored that pass through the channel at 0 delay time. Therefore, the 0-delay-time channel will be added to the direct monitors after the correlation for a group of channels with equal width. For example, the 0-delay-time channel of 1.5625 ns will be added to the direct monitor for channels 1-64 every 1.5625 ns. The 0-delay-time channel of 3.125 ns will be added to the direct monitor for channels 65-96 every 3.125 ns, etc. All correlation function and monitors are calculated according to eqn. (2.3.1)-(2.3.3).

For the calculation of the autocorrelation function, every channel is multiplied according to its delay time by a channel at zero delay time that possesses the same sampling time. For example, channels 1-64 (*i.e.*, delay times 0-100 ns, sampling time 1.5625 ns) are multiplied by the intensity signal that is presently measured during 1.5625 ns (*i.e.*, delay time zero, sampling time 1.5625 ns). By the same token, channels 65-96 are multiplied by the intensity signal that is presently measured during 3.125 ns. The results of the multiplication are summed up over time for the calculation of the autocorrelation. The counts of the sample at delay time 0 with sampling times of 1.5625 ns, 3.125 ns, *etc*. are summed up in the direct monitor M_{dir} of each group of channels with equal sampling time. The autocorrelation is then calculated by

$$G_i(m\Delta\tau_i) = \frac{\frac{1}{M-m}\sum_{k=1}^{M-m} n(k\Delta\tau_i)n(k\Delta\tau_i + m\Delta\tau_i)}{M_{dir,i} \cdot M_{del,i}} \quad , \qquad (2.3.1)$$

with

$$M_{del,i} = \frac{1}{M-m}\sum_{k=m+1}^{M} n(k\Delta\tau_i) \qquad (2.3.2)$$

and

$$M_{dir,i} = \frac{1}{M-m}\sum_{k=1}^{M-m} n(k\Delta\tau_i) \quad . \qquad (2.3.3)$$

Here, m is an integer, $\triangle\tau_i$ is the sampling time (*i.e.*, channel width) of channel I, and $m\triangle\tau_i$ is the delay time. M is the number of measurements over a period of $\triangle\tau_i$, and is given by $M = T/\triangle\tau_i$, where T is the total measurement time. $n(k\triangle\tau_i)$ is the number of photons at time $k\triangle\tau_i$, sampled with a channel width of $\triangle\tau_i$, and $n(k\triangle\tau_i + m\triangle\tau_i)$ the number of photons at time $m\triangle\tau_i$ later. M – m is the number of possible products $n(k\triangle\tau_i)n(k\triangle\tau_i + m\triangle\tau_i)$ over which the summation extend in eqn. (2.3.1)-(2.3.3). The autocorrelation function is symmetrically normalized with the direct and delayed monitors M_{dir} and M_{del} of corresponding channel i, respectively.

According to **Schwartz**'s inequality in eqn. (2.3.4), one should find that the autocorrelation value G(0) time would become one when the signal is invariable.

$$\left|\lim_{N\to\infty}\frac{1}{N}\sum_{j=1}^{N}Y_jY_j\right|^2 \le \left[\lim_{N\to\infty}\frac{1}{N}\sum_{j=1}^{N}Y_j^{\,2}\right]\left[\lim_{N\to\infty}\frac{1}{N}\sum_{j=1}^{N}Y_j^{\,2}\right] = \left[\lim_{N\to\infty}\frac{1}{N}\sum_{j=1}^{N}Y_j^{\,2}\right]^2 \qquad (2.3.4)$$

Here, we use two simple examples to illustrate the main idea of autocorrelation function: Supposing we measure two different forms of signal that are $n_1 = (1,1,1,1,1,1,1,1,1,1)$, and $n_2 = (1,4,7,2,3,8,0,7,-1,2)$ respectively, then the autocorrelation value at zero delay time could be calculated as

$$G(0)\big|_{n_1} = \frac{M\sum_{k=1}^{M} n(k\Delta\tau)n(k\Delta\tau)}{(\sum_{k=1}^{M} n(k\Delta\tau))^2} = 1$$
$$G(0)\big|_{n_2} = \frac{M\sum_{k=1}^{M} n(k\Delta\tau)n(k\Delta\tau)}{(\sum_{k=1}^{M} n(k\Delta\tau))^2} \approx 1.8 \qquad (2.3.5)$$

These values we obtained from eqn. (2.3.5) imply that the autocorrelation value at small delay time is an indication of the variation of the signals, in other words, the autocorrelation function would not decay once the input signal stays constant. However, there are several factors that characterize the variation of the signals, such as the statistical distribution, the mean value and the varience of the signals, etc. It would hard to tell which factor dominates the autocorrelation value at zero delay time unless one derive the specific relation in the system.

2.3.1 Statistical Accuracy of the Correlation Measurements of Scattered Light

The knowledge of the correct standard deviation is necessary for an accurate data evaluation, especially when fitting theoretical models to experimental data. However, the standard deviation in correlation spectroscopy has been mostly neglected in applications because of the difficulty in deriving its analytical calculation [15]. To

date, the standard deviation has been calculated mostly according to Koppel's equation. Koppel's equation was derived for the case of exponential autocorrelations. That is to say, it is not a universal solution. Despite all these, we could use the nature of statistics to obtain reliable data. Generally speaking, for each correlation value with different delay time it requires over 10,000 times of measurements for averaging in order to reach a statistical uncertainty lower than 1% [17]. Taking the response time of liquid crystals, laser stability, and the advantage of multiple tau technique into account, we set the whole measurement time to be 30 minutes in the following experiments.

Having attained the basic concepts of multiple tau correlation in section 2.3, we can now proceed with the estimation of statistical accuracy. The correlation value at different delay time, shown in Fig. 2.3.1, adds a new datum and takes an average every sampling time. Therefore, we can easily calculate the times for average at each delay time within 30 minutes by using the following equation:

times to be averaged = (total measurement time T – delay time of each channel) /sampling time of each group $\triangle\tau_i$.

The results are tabulated below, which implies that for a measurement of an autocorrelation curve that takes 30 minutes only the correlation values at delay time shorter than 10 seconds are counted as reliable.

	1sec	10sec	100sec
Times averaged	68664	8564	1014

Table 2-3-1 times for average at delay time 1, 10, 100 sec, respectively

2.4 Simulation Results

The stochastic differential equation that has been derived step by step in section 2.2 is also used as the primary equation for simulation.

$$\frac{d\psi(t)}{dt}+\frac{1}{\tau}\psi(t)=\sqrt{c}\Gamma(t) \tag{2.4.1}$$

and

$$\tau=\frac{\eta}{\widetilde{K}}=\frac{\eta}{\mathrm{K}\sin^2\theta(\frac{\pi}{d})^2} \quad . \tag{2.4.2}$$

In the following context, we would like to discuss how these two parameters, c and $\frac{1}{\tau}$ affect the fluctuations of φ angle in a SSFLC cell.

Let us begin by increasing the parameter c while setting $\widetilde{K}$ to be zero. In eqn. (2.4.1), $\widetilde{K}$ acts like an elastic constant. That is to say, the molecule with $\widetilde{K}$ been zero can be treated as a suspension particle in a liquid. The simulations of trajectory are shown bellow

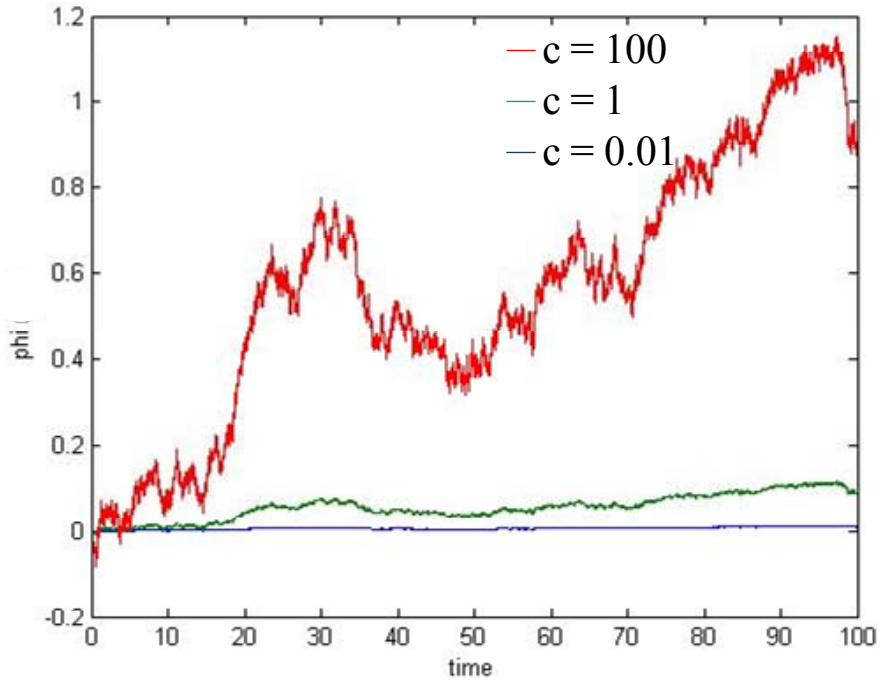

Fig. 2-4-1 The simulation results with eqn. (2.4.1) by fixing $\widetilde{K}$ parameter at zero. The red, green, blue lines represent the resulting trajectories of ϕ. Here c denotes the strength of thermal excitation.

The above results are consistent with our expectation. As the thermal excitation strength increases, the excitation force would push the particle further away from its original position. Because of the lack of elastic interaction ($\widetilde{K}$=0), the particle would never return to the places where it has once passed through.

Let us now fix the parameter ***c*** while increasing $\frac{1}{\tau}$ gradually. Since $\widetilde{K}$ acts like a restoring force, we figure that the molecule would behave more and more like an oscillator as the parameter $\frac{1}{\tau}$ becomes larger. Here, we have chosen the magnitude of thermal force ***c*** to be 1. The outcomes are depicted as follows

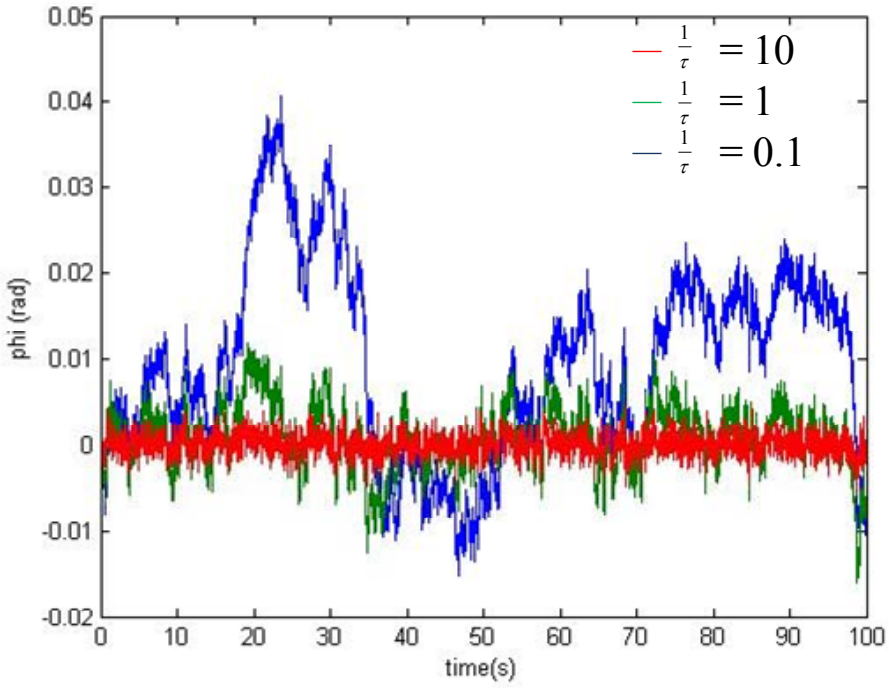

Fig. 2-4-2 The simulations of SSFLC cell with different $\frac{1}{\tau}$, while the thermal excitation strength ***c*** fixing at 1. Here τ is understood as a relaxation time. The red, green, blue lines represent the corresponding trajectory of ϕ.

Just as we have expected, the FLC molecules with higher values of $\frac{1}{\tau}$ (*i.e.*, the ratio of $\widetilde{K}$ to η) move forward and back across the equilibrium orientation with ϕ=0 while those with lower ratio relax slowly towards the equilibrium orientation. A more detailed description along with experimental data will be presented in the next chapter.

Chapter 3

Dynamic Light Scattering from Defect-Free SSFLC with Varing Doping Level of ZnO nanocrystals

3.1 The motivation of doping nc-ZnO

One nanometer is a magical point on dimensional scale. Nano-composites are at the confluence of the smallest of human-made devices and the largest molecules of living systems. Nanoparticles at this dimension scale embedded in a liquid crystal do not significantly perturb the director field in the liquid crystal, and interaction between the nanoparticles is weak. However, the nanoparticles may share their intrinsic properties with the liquid crystal via alignment and anchoring with the liquid crystal. For instance, that dispersing low concentrations of submicron ferroelectric particles in a nematic liquid crystal enhances the dielectric response and induces a linear response to the electric vector **E**. In contrast to molecular additives, these particle dispersions substantially lower the operating voltage of liquid crystal displays and related devices [18].

Our research was inspired by many previous publications that describe the peculiar behaviors of smaller particles embedded in liquid crystal matrices [19, 20],

calling for the need of a concerted research effort in nanostructured materials and liquid crystals. It has been employed to demonstrate the potential to yield an improved LC alignment and the electro-optical properties [21]. The developments has also revealed that the phase transition [22], ionic effect [23], and dielectric anisotropy [22] of liquid crystals are adjustable with doping of various nanomaterials, such as silica particles, LC-covered Pd particles [24], and ferroelectric nanoparticles, *etc*. The design parameters of the methodology include material, size and shape, doping concentration and surfactant properties of nanoparticles, which could provide an effective and flexible way to generate promising materials for the next generation liquid crystal application.

The material we choose to dope into FLC is Zinc oxide. It is a unique material that exhibits semiconducting and piezoelectric dual properties. With the special features, it has become a promising candidate for nanoelectronic and photonics. Compared with other semiconductor materials, ZnO having higher exciton binding energy (60 meV), is more resistant to radiation, and is multifunctional with uses in the areas as a piezoelectric, ferroelectric and ferromagnetic. So far, the various applications of ZnO nano materials such as biosensors, UV detectors and FED are under way.

To date, the mutual interaction between nanocrystals and liquid crystals is still a

profound mystery. However, through the light scattering experiment, we wish to come up with a possible model from a semi-microscopic view to describe the doping effect within the SSFLC cells. Furthermore, we would discuss its possibility to enhance application properties of a FLC material.

3.2 Material Properties of Ferroelectric Liquid Crystal Felix017/100

3.2.1 Material Properties of ferroelectric liquid crystal Felix017/100

The liquid crystal we used is a temperature-sensitive material that covers a variety of phases as listed in Table 3.2.1.

Phase transition (state)	Critical temperature (℃)
Isotropic ⟷ Nematic	87-84℃
Nematic⟷ Smectic-A	77℃
Smectic-A⟷Smectic-C*	73℃
Smectic-C*⟷ crystal	-28℃

Table 3-2-1 The phase transition temperatures of the ferroelectric liquid crystal Felix017/100 used in this study.

Among them, the electro optical properties in a smectic-C* phase are especially temperature dependent and thus they make a great impact on thermal experiments. Table 3.2.2 shows some properties that are needed for simulation.

Temperature (˚K)	Rotational viscosity (10^{-3}Pas · s)	Effective cone Angle θ (˚)	Spontaneous Polarization (nC/cm^2)
308˚K	105	14	47
318˚K	60	13	39
328˚K	35	11.5	32
338˚K	20	10	25

Table 3-2-2 The material parameters needed for the study with respect to temperature.

3.2.2 Sample preparation of Defect Free SSFLC with nc-ZnO doping

The defect-free surface-stabilized ferroelectric liquid crystal cells consist of two ITO-glass plates. The plates were coated with polyimide alignment layers (RN1182 from Nissan Chemical), which were rubbed in anti-parallel to suppress the occurrence of zigzag defects [25], and then separated by 1.5 μm-thick spacer to maintain a cell

gap approximating to the half-wave thickness $d_{\lambda/2} = \lambda/2\Delta n \simeq 1.9\mu m$ estimated with $\Delta n \simeq 0.17$ and λ=0.633μm.

Colloidal ZnO nanoparticles were prepared by the procedures that have been published in previous reports [26]. It is caped with 3-(trimethoxysily1) propy1 methacrylate (TPM) during the synthesis process of nc-ZnO. The corresponding bandgap as well as the photoluminescence peak were found to be 3.54eV and 518 nm, indicating the average diameter of the ZnO nanoparticles to be about 3.2 nm.

To prepare *nc*-ZnO doped SSFLC, we dispersed an appropriate amount of *nc*-ZnO nano powder into Felix 017/100 (purchased from Clariant incorporation in Germany) with ultrasonic at 85^{o}C for 40 min and then cooled down to room temperature in vacuum. To achieve various doping level of nc-ZnO, a weight percentage must be calculated precisely. The desired FLC material was filled into the test cells while it is in isotropic phases and then cooled down slowly to 35℃ to form a stable smectic-C* phase.

3.3 Experiment Results and Discussion

The measured results are shown below with an order of a SSFLC cell with different doping percentage of nc-ZnO from zero to five percent. In order to observe

the fluctuation caused by thermal, each of the cells was held at a series temperature from 35 to 65℃ and every other 10℃ in between, which falls on the smectic-C* phase temperature range of the liquid crystals we used. Let us first see the autocorrelation functions of pure SSFLC under different thermal excitation

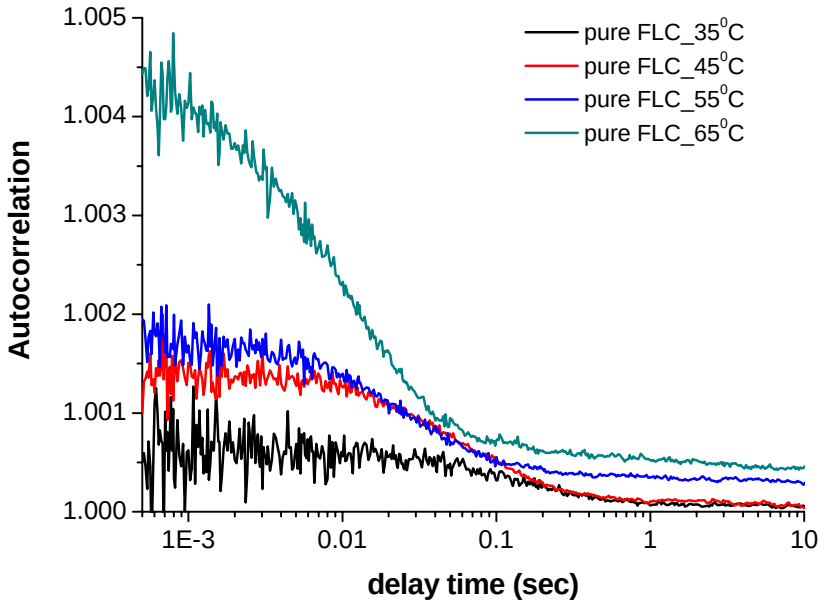

Fig. 3-3-1. The measured autocorrelation function of dynamic light scattering intensity from pure SSFLC at different temperature.

Let us first see the autocorrelation functions of pure SSFLC under different thermal excitation shown in Fig. 3.3.1. There are two distinct trends: for one thing, the autocorrelation function decays rapidly when temperature rises up. This phenomenon is reasonable and consistent with our previous analysis in chapter two, which also implies that we should gradually increase the parameter of random force c in

simulation as the temperature rises up. Therefore, the autocorrelation function drops faster to 1, reflecting the state of completely uncorrelated. To be more specific, the more random the system gets, the time duration from correlated to uncorrelated becomes shorter. The other characteristic we can easily observe is the autocorrelation value, which could be explained theoretically by using the eqn. (2.3.1) - (2.3.3) and is given by the following deduction. First, let us begin with eqn. (2.2.21)

$$\frac{d\psi(t)}{dt} + \frac{1}{\tau}T(t) = \sqrt{c}\Gamma(t). \tag{3.3.1}$$

Where $\frac{\eta}{\widetilde{K}} = \tau$ and $\widetilde{K} = K\sin^2\theta(\frac{\pi}{d})^2$. The solution to eqn. (3.3.1) is

$$\psi(\mathrm{t}) = \mathrm{N}\left(\phi_0 \mathrm{e}^{-\mathrm{t}/\tau}, \frac{\mathrm{c}\tau}{2}(1-\mathrm{e}^{-2\mathrm{t}/\tau})\right) \tag{3.3.2}$$

We could therefore calculate the correlation value at delay time zero $ACF(\tau = 0)$ by calculating first

$$\begin{aligned} &<\cos^2\psi(t)\cos^2\psi(t)> = <\cos^4\psi(t)> \\ &= \int_{-\infty}^{\infty}\cos^4\psi \cdot \frac{1}{\sqrt{2\pi\frac{c\tau}{2}}} \cdot e^{-\frac{\psi^2}{c\tau}} d\psi \\ &= \frac{1}{\sqrt{2\pi\frac{c\tau}{2}}}\left(3 + 4e^{-2(\frac{c\tau}{2})^2} + e^{-8(\frac{c\tau}{2})^2}\right). \end{aligned} \tag{3.3.3}$$

And the normalization factor

$$
\begin{aligned}
&< \cos^2 \psi(t) >^2 = \\
&= \left(\int_{-\infty}^{\infty} \cos^2 \psi \cdot \frac{1}{\sqrt{2\pi \frac{c\tau}{2}}} \cdot e^{-\frac{\psi^2}{c\tau}} d\psi \right)^2 \\
&= \frac{1}{8}(1 + e^{-2(\frac{c\tau}{2})^2})^2
\end{aligned}
\tag{3.3.4}
$$

Eqn. (3.3.3) and eqn. (3.3.4) lead to

$$
\begin{aligned}
ACF(\tau' = 0) &= \frac{< \cos^2 \psi(t) \cos^2 \psi(t+\tau)|_{\tau=0} >}{< \cos^2 T(t) >^2} \\
&= \frac{\frac{1}{\sqrt{2\pi \frac{c\tau}{2}}} \left(3 + 4e^{-2(\frac{c\tau}{2})^2} + e^{-8(\frac{c\tau}{2})^2} \right)}{\frac{1}{8}(1 + e^{-2(\frac{c\tau}{2})^2})^2} \propto \frac{1}{c\tau} = \frac{\rho + \tilde{K}\tau^2}{2k_B T \tau^2}.
\end{aligned}
\tag{3.3.5}
$$

Intuitively, when a system gets more chaotic, the signals become noisier and result in a lower correlation value [27]. This is also in agreement with our deduction in eqn. (3.3.5), which shows that the correlation value is inverse proportional to chaos c. However, eqn. (3.3.5) involves with at least four parameters. Without the precise value of them, it would be hard to evaluate the autocorrelation value. Fortunately, we could obtain these values by simulation. The parameters we would need for simulation are random force c, $\tilde{K}$ and η. Though we may not know the precise value of c, we do know its trends when temperature rises up. Besides that, the material properties η of Felix017/100 is extremely sensitive to temperature as indicated in Table 3-2-2. It almost drops to half of its original value every 10℃ increasing. By substitution the material property into eqn. (3.3.5) and supposing the elastic constant

K does not vary abruptly with temperature, we would obtain the simulated autocorrelation values listed in table 3-3-1, where one could see the autocorrelation values gradually increase just as those of experiment data with increasing temperature. Furthermore, we use eqn. (3.3.1) as a fitting model for dynamic light scattering from pure SSFLC. The simulation results and related parameters used are given below

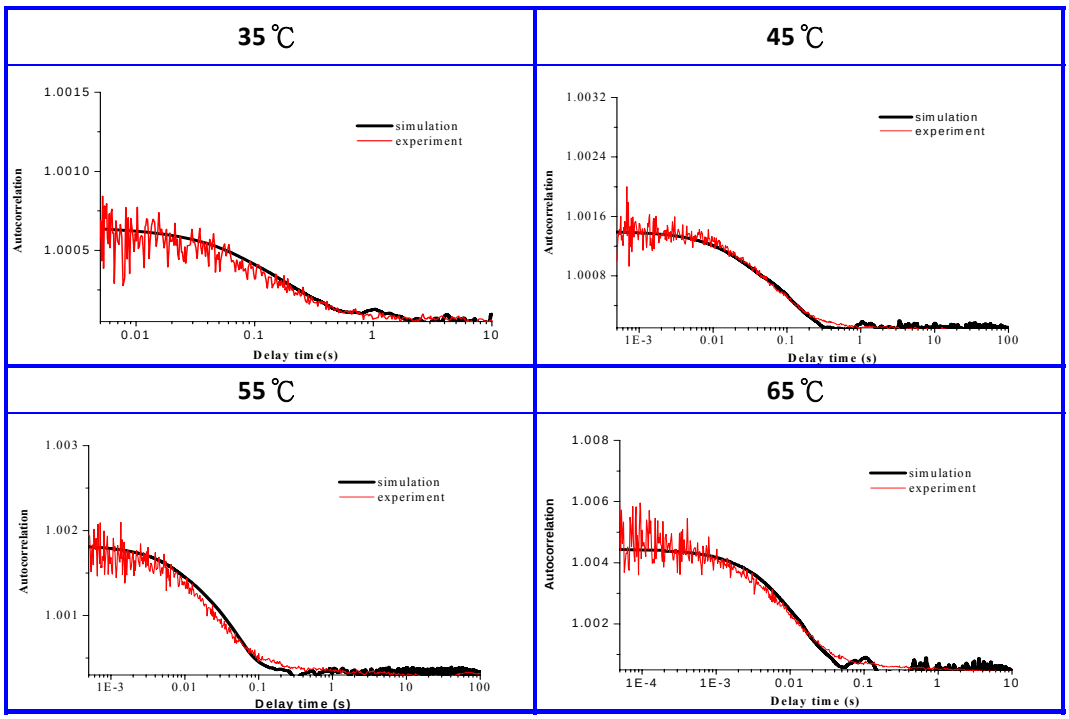

Fig. 3-3-2 The autocorrelation functions at a series temperature. The red curves represent the experiment data and the black lines are simulated from eqn. (3.3.1). The related parameters used in simulation are listed in table 3-3-1.

Temperature (°K)	Rotational viscosity (10^{-3}Pas · s)	$\tilde{K} = K\sin^2\theta(\frac{\pi}{d})^2$ (N/m^2)	$\frac{\eta}{\tilde{K}} = \tau$ (s^{-1})	C (dimesionless)	G(0) (dimesionless)
308°K	105	0.17	0.61	1.5	1.0699
318°K	60	0.15	0.4	2.1	1.46371
328°K	35	0.12	0.292	3.5	1.51
338°K	20	0.1	0.2	6	1.52

Table 3-3-1 The fitting parameters used in simulation.

The simulations in Fig. 3-3-2 do match the experiment results and the trend of parameter **c** that we expect to increase while temperature rises up is also in agreement with our experiment results.

To yield a better understanding, we further compared the four different doping levels of nc-ZnO under the same temperature. The corresponding autocorrelation functions acquired by the digital correlator hardware Flex02-01D are shown in the following figure.

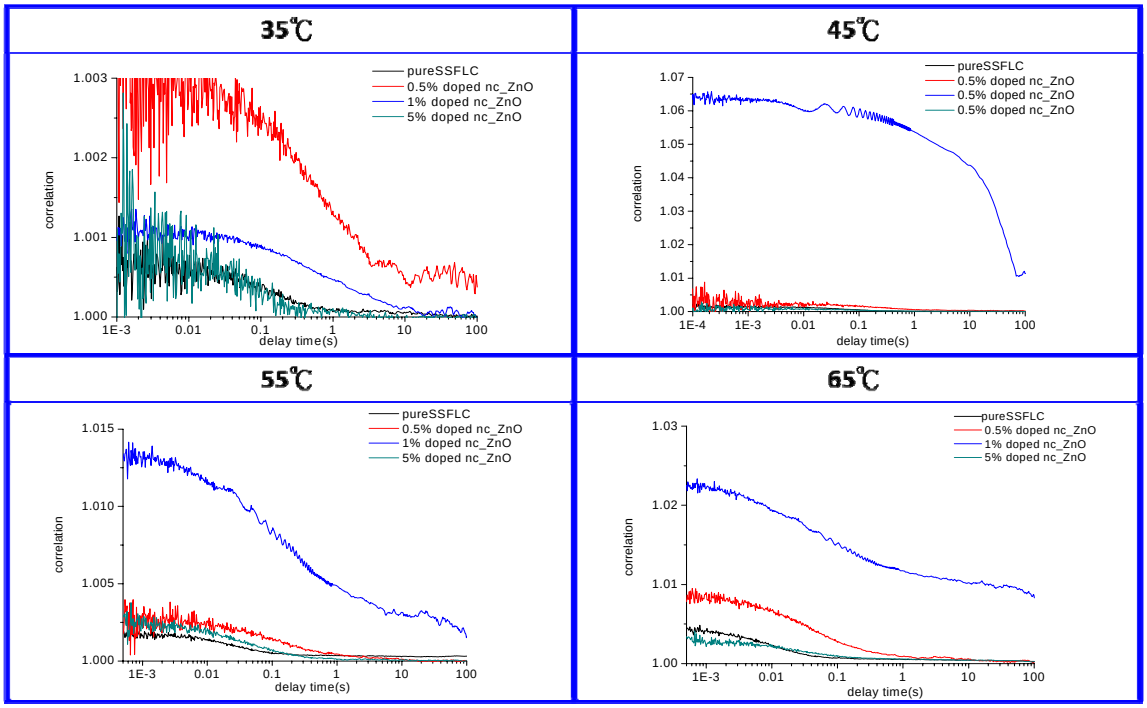

Fig. 3-3-2 The autocorrelation function of various doping level of nc-ZnO at 35, 45, 55, 65℃. The comparison at temperature 45℃ does not show clearly the variation between SSFLC cells of doping level 0, 0.5, 5% because of the scaling problem, and its zooming figure will be shown later in Fig. 3.3.3. The black, red, blue and green lines are the measured data of pure SSFLC, 0.5% doped nc-ZnO, 1% doped nc-ZnO and 5% doped nc-ZnO, respectively.

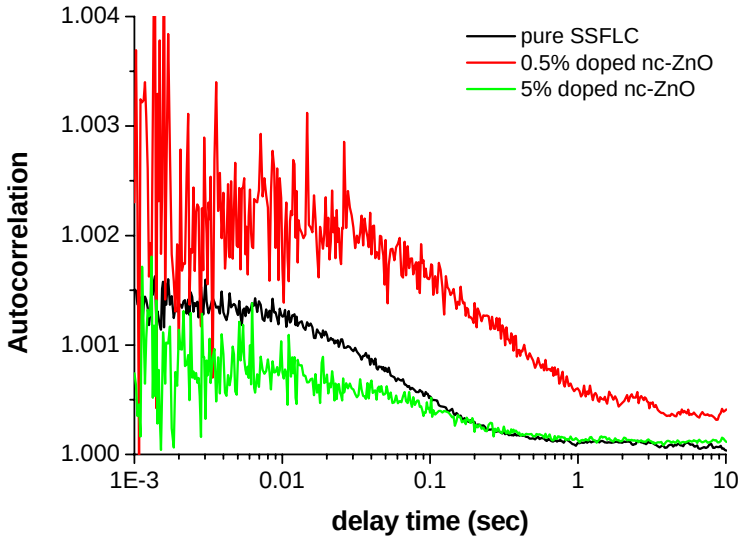

Fig. 3-3-3 The zooming picture of SSFLC cells with 0%, 0.5% and 5% doped nc-ZnO at 45℃. The black, red and green lines represent the measured raw data of 0%, 0.5% and 5% doped nc-ZnO, respectively.

The comparisons give some surprising results: (1) The autocorrelation functions of SSFLC with doping level 0%, 0.5%, 5% of nc-ZnO have two things in common－when the temperature rises up (a) the time duration from correlated to uncorrelated shorten. (b) The correlation value at small delay time increases. These two features are attributed to the abruptly changes in viscosity η as is deduced previously. (2) The measured raw data of doping level of 1% nc-ZnO have showed a very unique behavior from the others. As one could easily tell that at temperature 45, 55, 65℃ this SSFLC cell exhibits an oscillation in the autocorrelation function while none of the other cells does. (3) Except for the data of SSFLC with doping level of 5% nc-ZnO (the green lines), the other data with doping nc-ZnO (*i.e.*, the red and blue lines) have larger autocorrelation values at small delay time and longer time duration from correlated to uncorrelated than those of pure SSFLC's (black lines) measured data. (4) The measured raw data of SSFLC with doping level of 5% nc-ZnO are very close to those of pure SSFLC. That is to say, the black lines at temperature 35, 45, 55 and 65℃ are almost identical to the green ones in magnitude and trends. Combining the fact with eqn. (2.2.23) and eqn. (3.3.5), we would discover that doping 5% nc-ZnO into SSFLC probably does not affect much the macroscopic property of SSFLC such as viscosity η and the elastic constant K so that the autocorrelation

values and the duration time from correlated to uncorrelated stay unchanged.

Let us now try to explain these observations presented above. Recall that in section 1.3, we described the smectic phase to have more spatial order than nematic phase does, which is revealed by a fact that the smectic phases has somewhat positional order while the nematic does not. This fact strongly suggests that the dynamical behavior in the smectic phase structure is supposed to be closer to that in the solid crystal structure than that in the nematic phase structure. But unlike the underdamped dynamics of the phonons in the solid crystal, molecular fluctuations in the ferroelectric liquid crystals are still overdamped as proved in the autocorrelation function measured with the undoped SSFLC cell shown in Fig. 3.3.1. However, something interesting happened right after we doped 1% nc-ZnO into the pure SSFLC cell which then exhibit oscillation in its autocorrelation. With the knowledge in mind, we turn ourselves back to eqn. (2.2.13) and analyze it with

$$\rho\frac{\partial^2\phi}{\partial t^2}+\eta\frac{\partial\phi}{\partial t}+K\sin^2\theta\frac{\partial^2\phi}{\partial y^2}=\overline{F}_{thermal}, \tag{3.3.6}$$

Again, we employed the separation of variables to extract the dynamical part of the equation

$$\rho\frac{\partial^2\psi(\mathrm{t})}{\partial t^2}+\eta\frac{\partial\psi(t)}{\partial t}+K\sin^2\theta(\frac{\pi}{d})^2\psi(t)=F_{thermal}(t) \tag{3.3.7}$$

Defining the angular velocity ω and $\alpha^2=\dfrac{K\sin^2\theta(\frac{\pi}{d})^2}{\rho}$, we derive [28]

$$\begin{cases} d\psi = \omega(t)dt \\ dw = -\dfrac{K\sin^2\theta(\dfrac{\pi}{d})^2\psi(t)}{\rho}dt - \dfrac{\eta}{\rho}\omega(t)dt + \widetilde{F}_{thermal}(t)dt \end{cases} \tag{3.3.8}$$

$$\Rightarrow d\begin{pmatrix}\psi\\ \omega\end{pmatrix} = \begin{pmatrix} 0 & 1 \\ -\alpha^2 & -\dfrac{\eta}{\rho}\end{pmatrix}\begin{pmatrix}\psi\\ \omega\end{pmatrix}dt + \begin{pmatrix} 0 \\ \widetilde{F}_{thermal}(t)dt\end{pmatrix}.$$

The characteristic equation of the matrix

$$\mathrm{A} = \begin{pmatrix} 0 & 1 \\ -\alpha^2 & -\dfrac{\eta}{\rho}\end{pmatrix} \tag{3.3.9}$$

is $\mu^2 + \dfrac{\eta}{\rho}\mu + \alpha^2 = 0,$ with the eigenvalues

$$\mu_1 = -\frac{\eta}{2\rho} + \sqrt{(\frac{\eta}{2\rho})^2 - \alpha^2}, \qquad \mu_2 = -\frac{\eta}{2\rho} - \sqrt{(\frac{\eta}{2\rho})^2 - \alpha^2}. \tag{3.3.10}$$

By using the theory of the harmonic oscillator, we distinguish three cases [28, 29]:

1. overdamped $\dfrac{\eta}{(\sin\theta\frac{\pi}{d})^2} > K$,

2. critically damped $\dfrac{\eta}{(\sin\theta\frac{\pi}{d})^2} = K$, (3.3.11)

3. underdamped $\dfrac{\eta}{(\sin\theta\frac{\pi}{d})^2} < K$.

From eqn. (3.3.11), we now understand that the dynamics of SSFLC from overdamped to underdamped can occur with the changes of the material properties. Furthermore, with the help of eqn. (3.3.5) and eqn. (2.2.25) we can recover the following three characteristic features that correspond to the experimental observations (2) and (3) by gradually increasing the parameters K:

(1) the smaller **c** parameter resulting in the longer time duration from correlated to uncorrelated;

(2) higher value of autocorrelation at small delay time; and

(3) the dynamical transition from overdamped to underdamped.

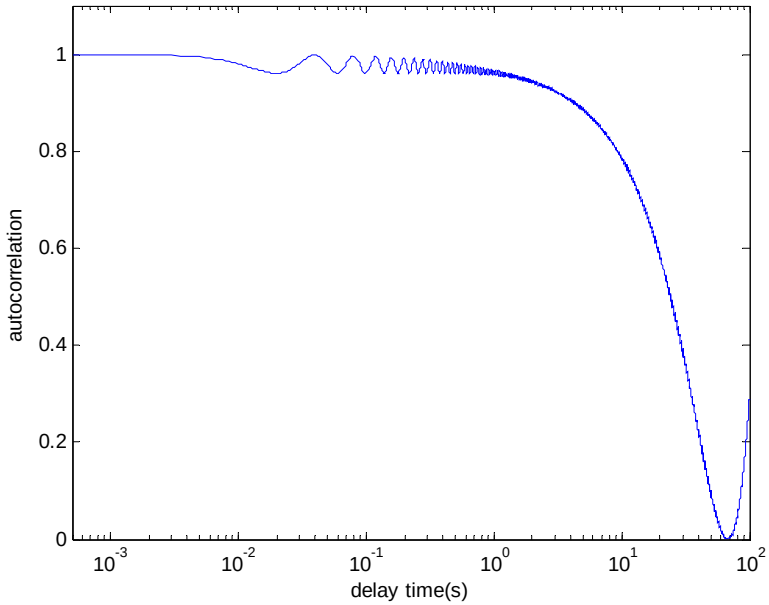

Fig. 3-3-4 A simulation result for underdamped dynamics. Note that the oscillation behavior begins at delay time 0.02 seconds, which equals to the experiment result of SSFLC doped with 1% ZnO at 45℃.

An underdamped simulation based on eqn. (3.3.7) is given above. Overall speaking, the doping with nc-ZnO somehow changes the material properties such as K and η especially the former one which, on the other hand, is related to the order parameter [30]. To construct a possible mechanism of the doping effect, it might be better to begin with the interaction between the liquid crystals and ZnO crystals. Experimental and theoretical studies on ZnO crystals have all revealed a presence of a giant

permanent dipole moment that is about 4800 nC/cm^2 [31], which serves as a local electric field that would force the surrounding ferroelectric liquid crystals to align along its electric lines of force. As a consequence, the SSFLC doped with nc-ZnO have better spatial order [21, 30]. However, if the liquid crystals surrounded by a moderate amount of nc-ZnO (*i.e.*, a higher doping level of nc-ZnO) would not know how to align but to follow its nature's lead since the dipolar fields generated from each nc-ZnO are very likely to cancel one another. In short, it is because of the unchanged alignment that results in the unchanged material property and lead to similar results as those of pure SSFLC.

Chapter 4

Probing into the Influence of the Stochastic Processes on the Field-Driven Motion in SSFLC

4.1 Introduction

Many of the physical properties of mesomorphic materials, such as birefringence, optical activity, viscosity and thermal conductivity could be affected by varying external stimulations. Electric fields, magnetic fields, thermal and acoustical excitation can be invoked to induce material responses [32]. As illustrating in Figure 4.1 for the case of liquid crystal, efforts are focused on the electro-optic effect because of the ease and efficiency of LC excitation with an applied voltage as compared with other means of stimulation. However, many more possibilities can be explored further.

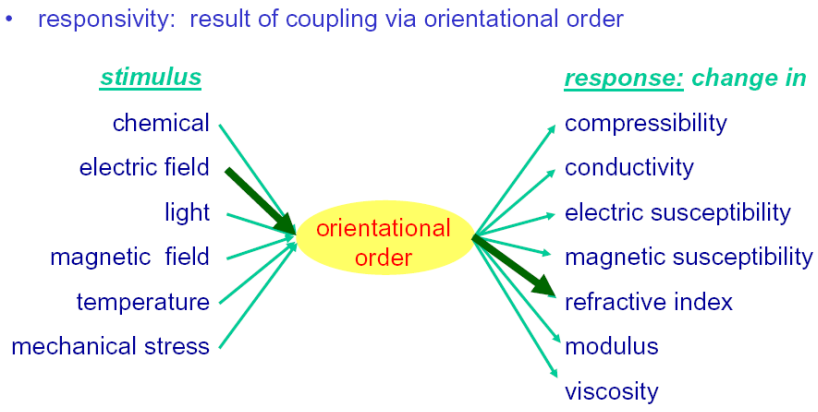

Figure 4-1-1 Responsivity of LC that can be coupled via LC orientational order.

Among these responsivities of mesomorphic materials, not many of them have been explored about how the spontaneous fluctuation interferes with a deterministic motion of the constituent molecules. Based on the kinetic theory, such a stochastic motion should always exist and accompany all kinds of activities within the substances at temperature above the absolute zero. It is also inevitable in a practical application, which may cause an unexpected result or error.

In this chapter, we shall first discuss how a random force perturbs deterministic excitation modes of FLC molecules excited by an external electric field. We will show the simulation results and compare them with the experimental investigation. Finally, we will examine how the coupling of the field-driven motion in SSFLC with the random fluctuation affected by doping of nc-ZnO.

4.2 Basic Equations

Let us go back to section 2.2, where we have derived a form of free energy suited for FLC in eqn. (2.2.12). The free energy is comprised of an elastic free energy and a coupling energy to an electric field, a dielectric free energy and a spontaneous polarization free energy.

$$\mathrm{E}_{free} = e_{elastic} + e_{dielectric} + e_{couple} \tag{2.2.14}$$

When an electric field is applied on a FLC cell, a dielectric torque occurs on the director and leading to a free energy $-\varepsilon_y E^2/2$. In addition, FLC possesses a nonvanishing spontaneous polarization, which can couple to the electric field and causes a free energy $-P_s E \sin\phi$ and determines the response time of electro-optic effect according to [33]

$$\tau_r \sim \frac{\eta}{P_s \cdot E} \quad , \tag{4.2.1}$$

where, η is rotational viscosity for the director motion on the cone of the tilt angle. If the principal dielectric constants along $\vec{n}$, $\vec{P}$ and $\vec{P}\times\vec{n}$ are ε_3, ε_2 and ε_1, respectively, the y-component (*i.e.*, the cell normal) of the dielectric tensor in xyz-coordinates can be expressed in the following form [30]

$$\varepsilon_y = (\varepsilon_1 \cos^2\theta + \varepsilon_3 \sin^2\theta)\sin^2\varphi + \varepsilon_2 \cos^2\varphi. \tag{4.2.2}$$

In response to an external electric field applied along the y-direction, the equation of motion in eqn. (2.2.14) becomes

$$\eta\frac{\partial\phi}{\partial t} = -K\sin^2\theta\frac{\partial^2\phi}{\partial y^2} + \frac{1}{2}\frac{\partial\varepsilon(\phi)}{\partial\phi}E^2 + P_s E\sin\phi + F_{thermal}$$

$$= -K\sin^2\theta\frac{\partial^2\phi}{\partial y^2} + \frac{1}{2}\sin 2\phi\sin^2\theta(\varepsilon_3 - \varepsilon_1)E^2 + P_s E\sin\phi + F_{thermal} \quad , \tag{4.2.3}$$

where the dielectric free energy was further simplified by assuming $\varepsilon_2 \approx \varepsilon_1$. This is an equation of both time and space dependence. However, the first term in the right hand side of the equation can be neglected due to the bookshelf geometry. The second

term compared with the third term is also negligible at low fields. Thus the equation can be reduced to

$$\frac{d\phi}{dt} = \frac{P_s E}{\eta}\sin\phi + \frac{1}{\eta}F_{thermal}(t) \tag{4.2.3}$$

F_{thermal} can be expressed in terms of stochastic mathematics as

$$F_{thermal}(t) = \eta\sqrt{c}\Gamma(t) = \eta\sqrt{c}\lim_{dt\to 0} N(0,\frac{1}{dt}) \quad . \tag{4.2.4}$$

Therefore, eqn. (4.2.3) becomes

$$\frac{d\phi}{dt} = \frac{P_s E}{\eta}\sin\phi + \sqrt{c}\Gamma(t) \quad . \tag{4.2.5}$$

Here, the term $\frac{P_s E}{\eta}$ not only determines the response time of the FLC, but also has a great impact on the molecular motion; as one can see from eqn. (4.2.3) that the stronger this coupling energy is, the more easily the FLC director be driven and results in a greater variation in ϕ. The second term on the right hand side of equality is the random force caused by thermal energy as introduced in Chapters two and three. We have two driving forces- one is a deterministic form, and the other one is characterized with a probability density. One must be curious about how the FLC molecules behave under the two forces. We will probe the dynamics through the simulation, and further verify it by comparing the simulation with experimental observations.

The parameters used in the simulation are as follows. The spontaneous polarization P_s = 47 nC/cm^2, cone angle 2θ = 55.1^o, cell thickness d=2μm, rotational

viscosity η = 105 mPas · S, dielectric constant ε = 5.65 and, above all, the magnitude of random force 0.5, for we hold the SSFLC at a temperature around 25℃.

4.3 Simulation Result

In order to reveal the influences of random force on the deterministic motions of FLC molecules, it is necessary to analyze first the dynamical behavior of the FLC molecules in absence of the random force. This can be achieved by turning off the random force and applying an electric field with a sinusoidal driving voltage (V_{pp}=1V) of 10Hz in eqn. (4.2.5). For a clear revelation, three different presentations are shown below: first, the simulation result of azimuthal angle φ based on the equation of motion derived in previous section (*i.e.*, eq. (4.2.2)) is presented; second, the zoom-in picture of the angle φ dynamics is shown for the dynamical detail; third, the corresponding light intensity autocorrelation function is given.

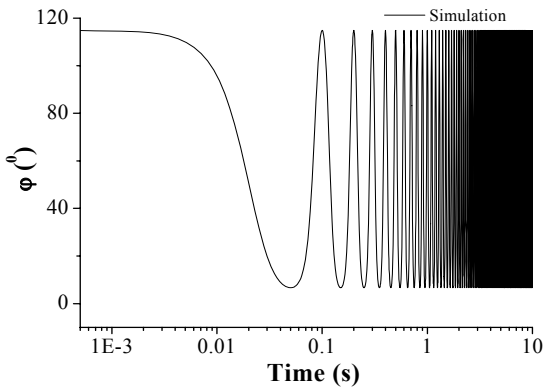

Figure 4-3-1(a) The simulated trajectory of angle φ with parameters c =0, Vpp=1V and

frequency at 10Hz.

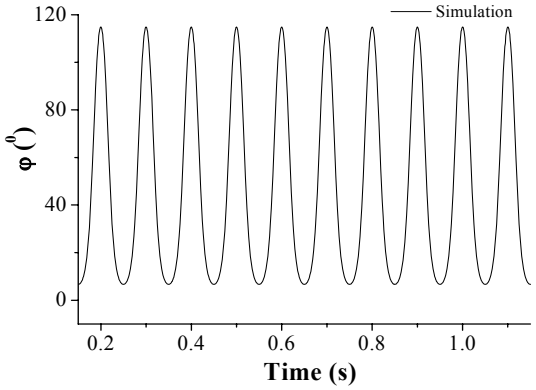

Figure 4-3-1(b) The zoom-in picture of figure 4-3-1(a)

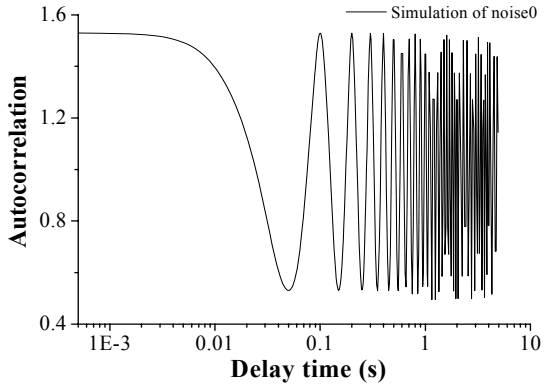

Figure 4-3-1(c) The corresponding autocorrelation

The first simulation shown above is the dynamics of SSFLC driven by a sinusoidal electric waveform of frequency 10Hz, which implies that the director of FLC molecules should oscillate with the electric field at the same frequency. That is, the director would vibrate 10 times in one second as seen in Fig. 4-3-1(b). In Fig. 4-3-1(a), we have also observed that the driving voltage, whose peak to peak equal to one volt, may not have the power to fully switch the director from 0 to π. But, the motion of the FLC molecules is correctly modulated with the external driving field as shown in Fig. 4-3-1(b). The frequency of the optic axis coming back and forth could

not only be determined from Fig. 4-3-1(b), but also be seen in its corresponding autocorrelation function (ACF), where the adjacent two peaks of the oscillation in Fig. 4-3-1(c) is about 0.1 seconds which is just the time the FLC molecules take to come back and forth to its original place. Moreover, the ACF shows everlasting amplitude of oscillation, which is beyond question for there is no other random force that could disrupt the deterministic path of FLC molecules so that the corresponding ACF remains the same throughout the process.

We now that know how the FLC molecules behave without the thermal disturbance, we would gradually increase the random force to see what might happen. The following simulation results are presented by increasing the random force from 0.1, 0.5, 1.2, and 2.5. Note that the value of 0.5 corresponds to a temperature of around 25℃.

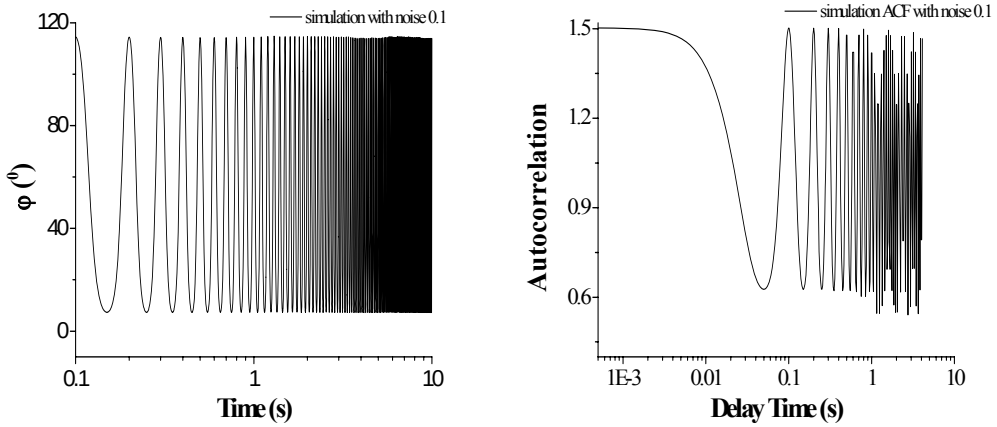

Figure 4-3-2(a): The φ trajectory and its corresponding ACF at parameters c=0.1, V_{pp}= 1V, and frequency 10Hz.

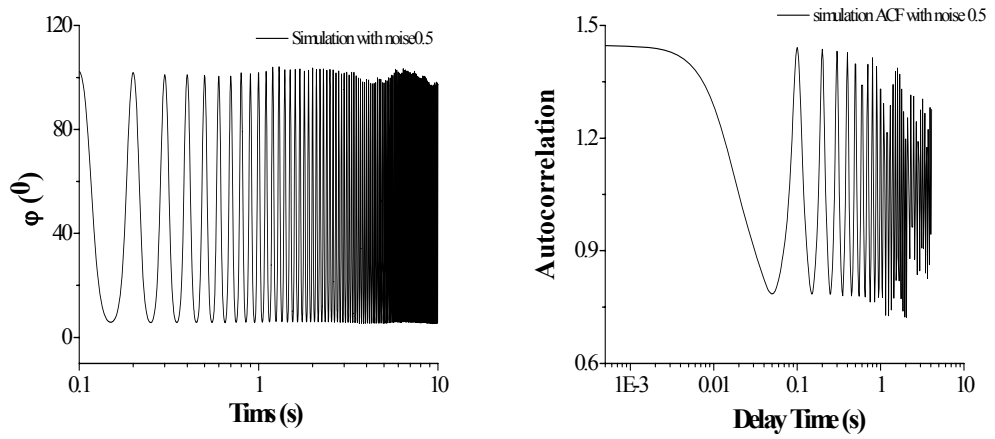

Figure 4-3-2(b): The φ trajectory and its corresponding ACF at parameters c=0.5, V_{pp}= 1V, and frequency 10Hz.

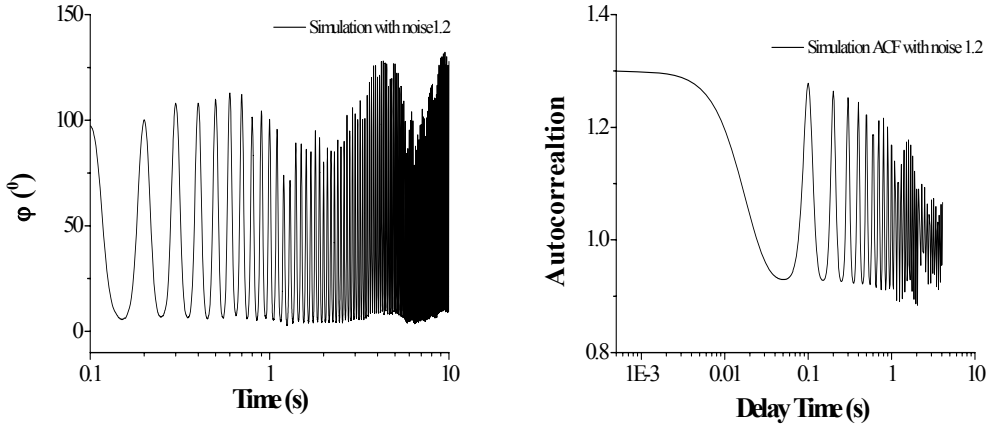

Figure 4-3-2(c): The φ trajectory and its corresponding ACF at parameters c=1.2, V_{pp}= 1V, and frequency 10Hz.

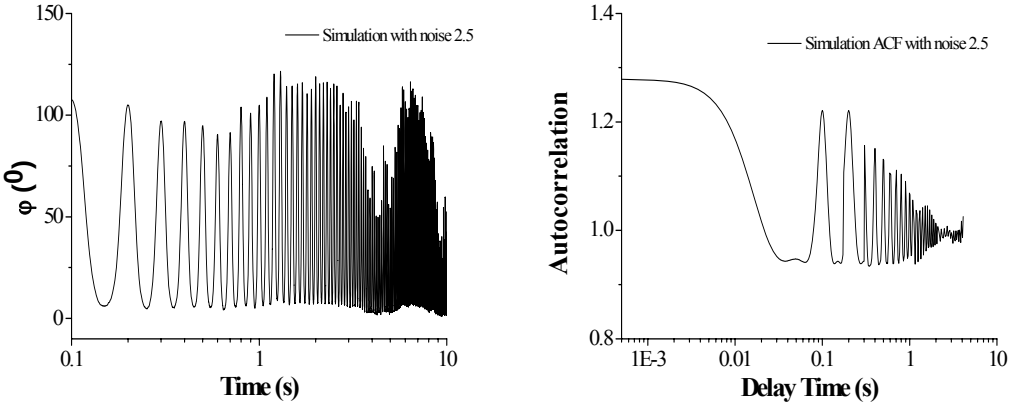

Figure 4-3-2(d): The φ trajectory and its corresponding ACF at parameters c=2.5, V_{pp}= 1V, and frequency 10Hz.

From the simulations shown in Figures 4-3-1 and 4-3-2, we can draw some

conclusions: when the random force increases (1) the trajectory of the director becomes more and more irregular. This is because the random force is a random variable and brings in the irregularity in the φ route even under a deterministic field; (2) there is a decrease in the autocorrelation value at delay time zero. This phenomenon is consistent with our intuition that the system should become less similar as it gets more and more chaotic; (3) the ACFs with the disturbing of a random force show decaying amplitudes at longer delay time. The reason of a decrease of amplitude is no other than the random force existing in the system, which makes the trajectory of motion more and more irregular and thus results in a less similarity with time in the ACF. To sum up, the dynamics under measure actually manifests itself in the corresponding ACF which, for a periodic motion, implies us the precise period and the degree of random force involved.

4.4 Experimental Study of the Dynamic Light Scattering from Pure SSFLC and Nanocrystalline-ZnO doped SSFLC

4.4.1 Experiment Results of Pure SSFLC

Having connected the electrodes attached on the ITO of the cell to a function generator, we apply one volt of sinusoidal driving voltages with a series of

frequencies from 10Hz to 10 kHz. The experimental results shown below are presented with different frequencies, and each of them would be compare with the simulation result under the same condition.

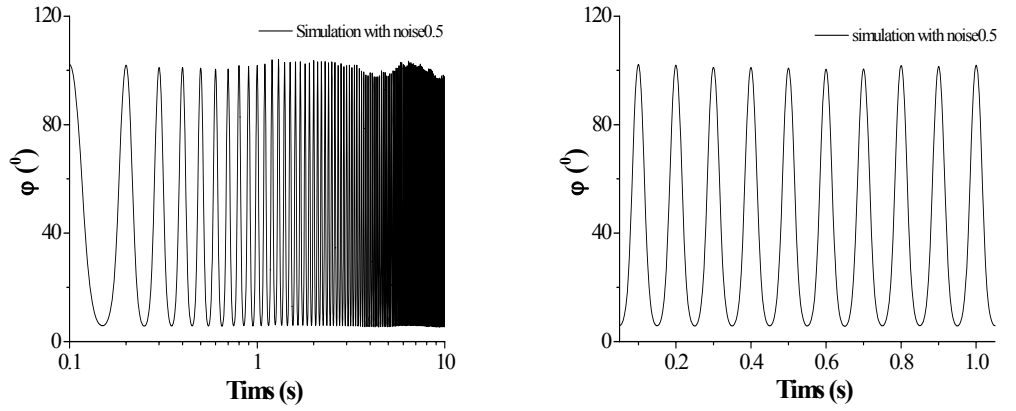

Figure 4-4-1(a): The simulated trajectory of angle φ with parameters c =0.5, Vpp=1V and frequency at 10Hz.

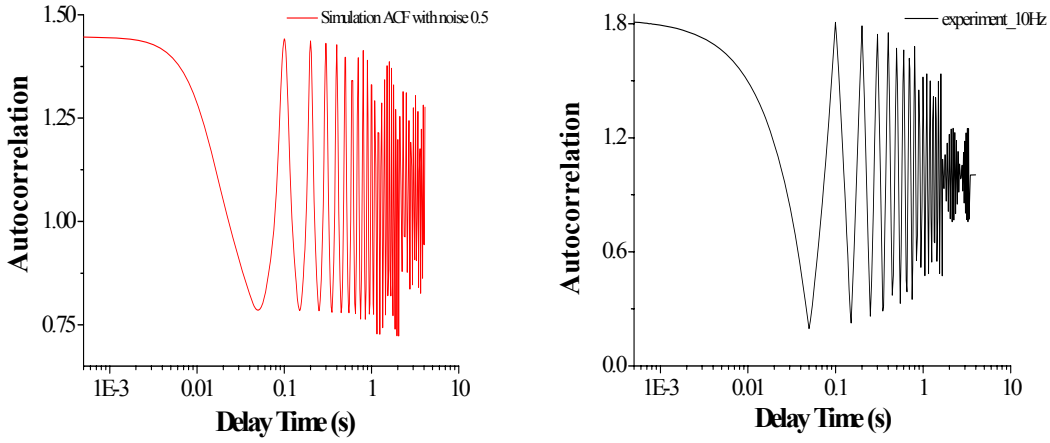

Figure 4-4-1(b): The comparison of the experimental and simulated ACFs by applying a sinusoidal driving voltage of 10 Hz. The picture on the left is the simulated result while the experimental curve is presented on the right hand side.

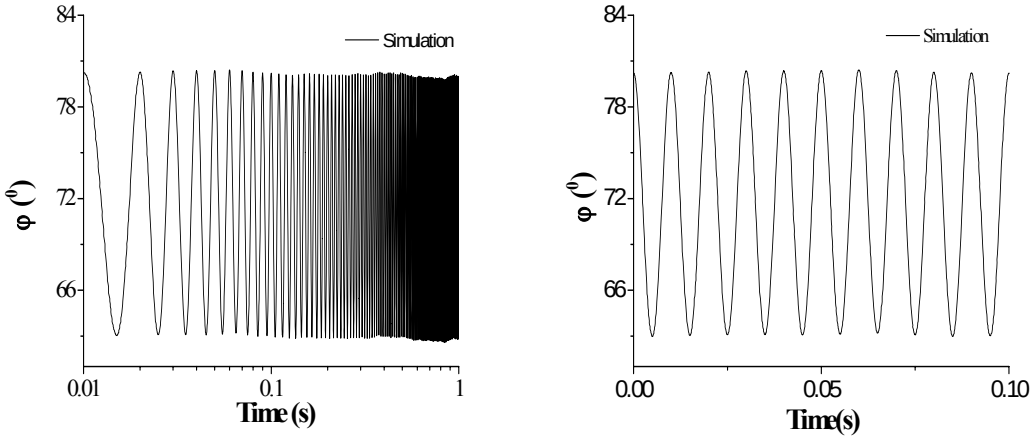

Figure 4-4-2(a): The simulated trajectory of angle φ with parameters c=0.5, V_{pp}=1V and frequency 100 Hz.

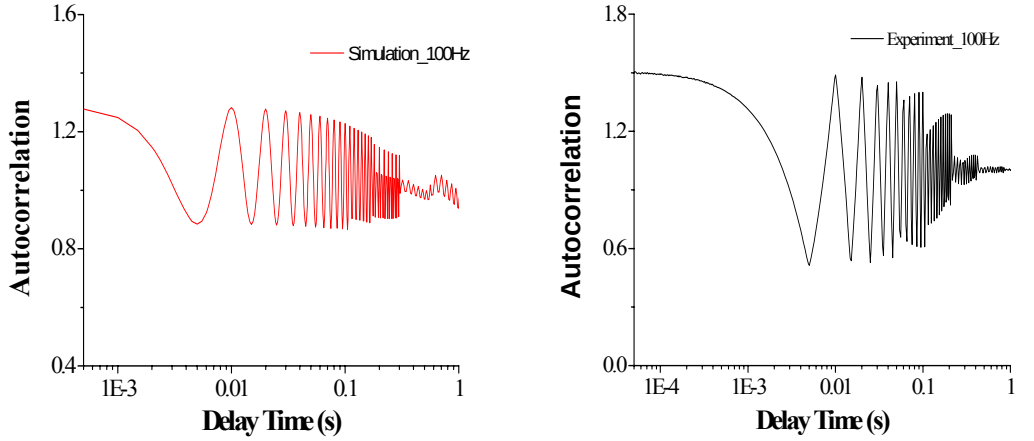

Figure 4-4-2(b) The comparison of experiment and simulated results by applying a sinusoidal driving voltage with 100Hz. Note that the frequency of the oscillation in ACF corresponds to the driving frequency. This is also the sign of the FLC molecules being modulated by the external field.

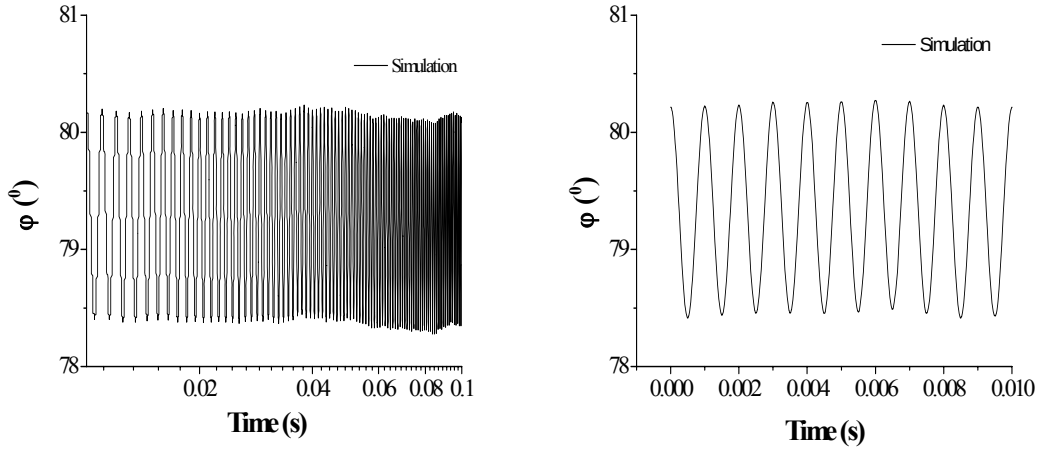

Figure 4-4-3(a): The simulated trajectory of angle φ with parameters *c* =0.5, Vpp=1V and frequency 1 kHz.

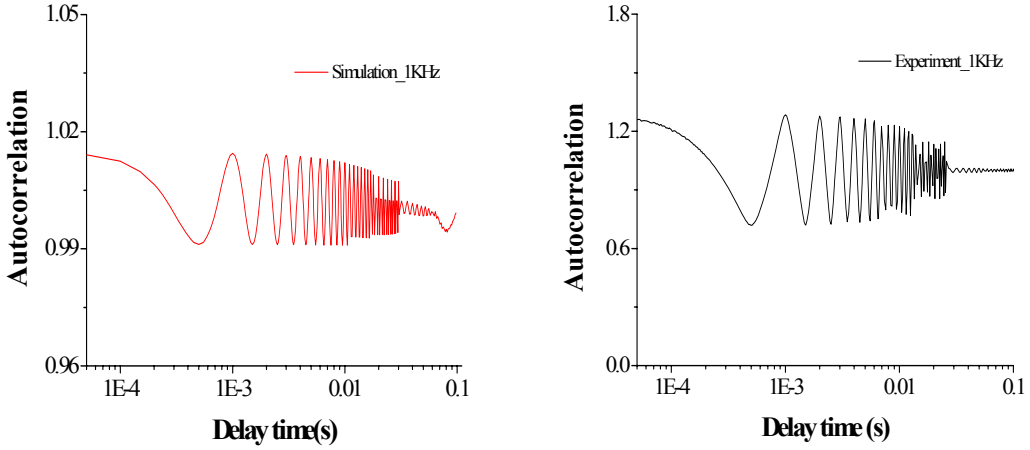

Figure 4-4-3(b): The comparison of the experimental and simulated ACFs by applying a sinusoidal driving voltage of 1kHz. The picture on the left is the simulated result while the experimental curve is presented on the right hand side. One can observe that the amplitude of oscillation in ACF is getting smaller as the driving frequency increases.

The three experiments share two things in common: (1) the FLC molecules driving by the electric field with 10 Hz to 1 KHz seem to catch up the field quite well; the temporal separation of two neighboring peaks in the ACFs indicates that the FLC

molecules truly move back and forth in response to the driving field. (2) According to our conclusion drawn in section 4.3, we are certain that the decay of amplitudes shown in the ACFs is due to the random force. However, there are also some distinct differences among them. First, the oscillating amplitude of the conic motion (*i.e.*, φ) of FLC decreases with the increasing frequency of the applied field. This is a reasonable outcome as the travelling distance of a forced motion is proportional to the lasting time of the applied field. Secondly, if we take a closer look at the ACFS, we can find that the more greatly the FLC director oscillates the bigger correlation value the ACF would become.

Let us increase the driving frequency to 10 kHz and study the resulting dynamics. The driving voltage is set to be V_{pp}=1V. According to eqn. (4.2.1), the FLC molecules may not be able to catch up anymore since the response time is longer than 100 μsec. The failure of FLC molecules to switch coercively with the external field could be revealed in the simulated trajectory of motion shown in fig. 4-4-4(a). In other words, instead of being modulated by the external driving field with such a high frequency and low driving voltage, the FLC molecules in a highly viscous environment practically remain at their original orientation. The little variation in the orientation of FLC director causes a nearly constant scattered light which in turn results in a flat autocorrelation function.

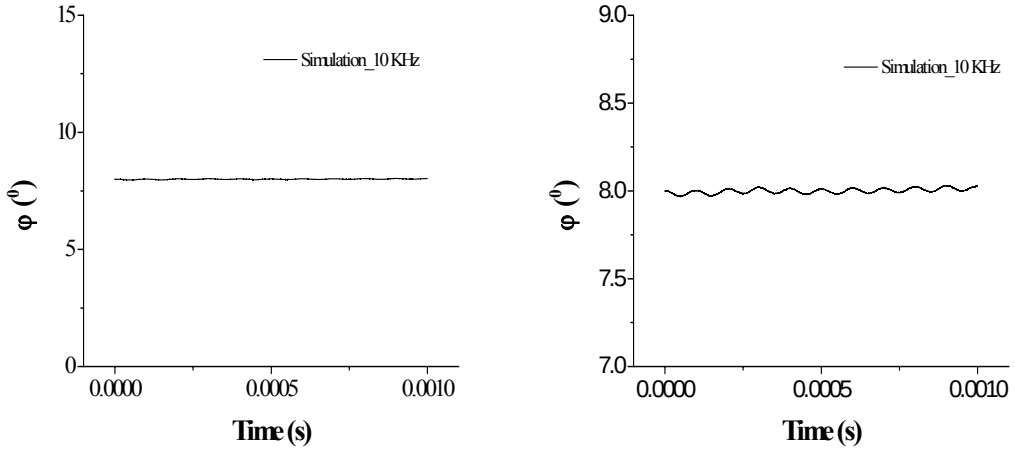

Figure 4-4-4(a): The simulated trajectory of angle φ with parameters c=0.5, V_{pp}=1V and frequency at 10 kHz.

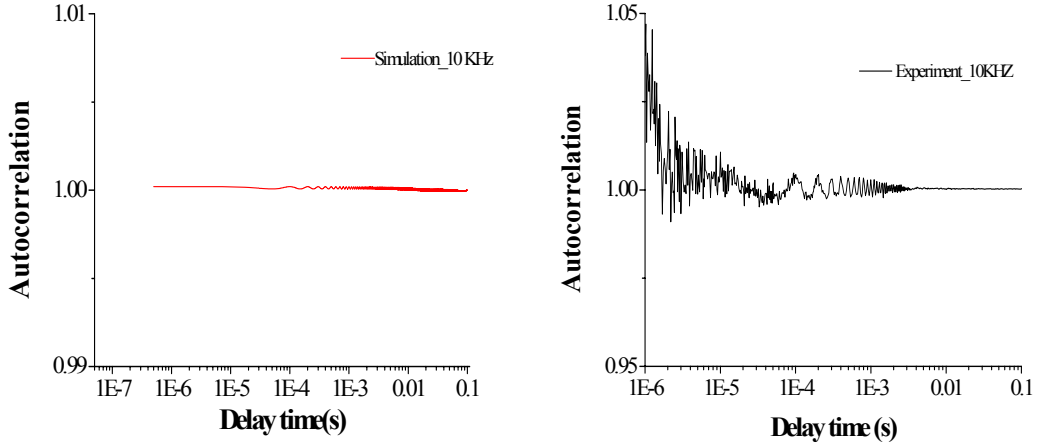

Figure 4-4-4(b): The comparison of experimental and simulated ACF curves by applying a sinusoidal driving voltage of 10 kHz. Both results show a weak orientational variation in the ACFs.

Based on the investigation, we can conclude: (1) the autocorrelation indeed reflects the dynamics under measure. For a periodic oscillating behavior, the temporal separation of the first two peaks in the autocorrelation function represents the time it takes to come back to the place closest to where it started and it is at this moment, the ACF reaches a maximum similarity. Therefore, the delay time between any of two

neighboring peaks in ACF corresponds to the oscillation period; (2) from both simulation and experimental results, the random force has proved to be nonnegligible; (3) the term $P_s E/\eta$ is an important electro-optic parameter, which governs the response time of FLC molecules as indicated by eqn. (4.2.1). The parameter can also serve as an indication of the molecular motion revealing in the ACF; the stronger the coupling energy is, the more intensive the molecules motion becomes and results in greater amplitude of oscillation in the corresponding ACF. These conclusions will help us understand the following results of doped SSFLC with nc-ZnO.

4.4.2 Experiment Results of SSFLC with various doping level of nz-ZnO

For a better understanding, we will show the experimental results with an increasing doping level from 0 to 5%, and each of them would contain data sets measured at four different driving frequencies 10Hz, 100Hz, 1 kHz, and 10 kHz. The corresponding autocorrelation functions are presented in fig. 4.4.2.

The dynamics of the four cells with different nc-ZnO doping levels exhibit one thing in common: the amplitudes of oscillation in ACFs gradually decay as the applied frequency increases. We believe that it is because the molecules do not have enough time to fully switch their states with such a low driving field but high frequency. This also implies that as the applied frequency increases, the director $\hat{n}$

rotates less and less around the cone axis and therefore leads to a smaller ACF in amplitudes. This observation once again confirms our simulation in section 4.3.

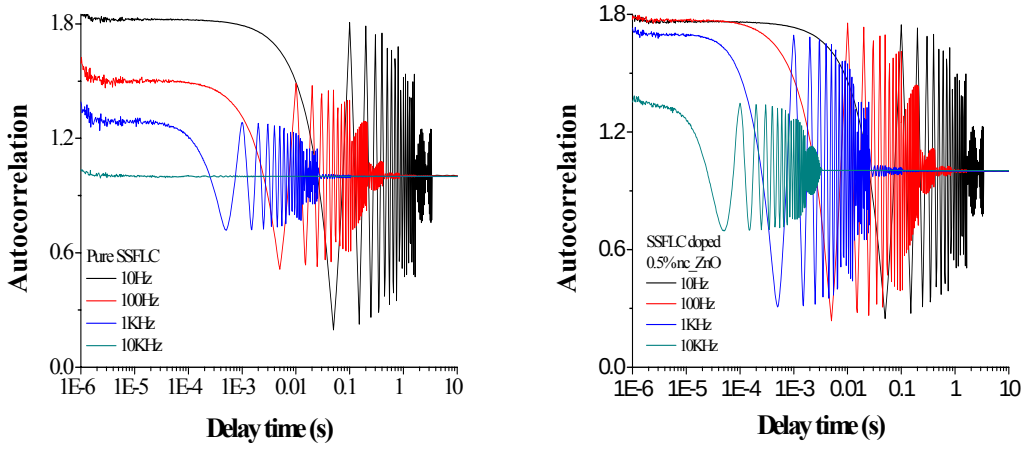

Figure 4-4-5(a): The corresponding autocorrelation function of SSFLC cells doped with 0 (left panel) and 0.5% (right panel), respectively.

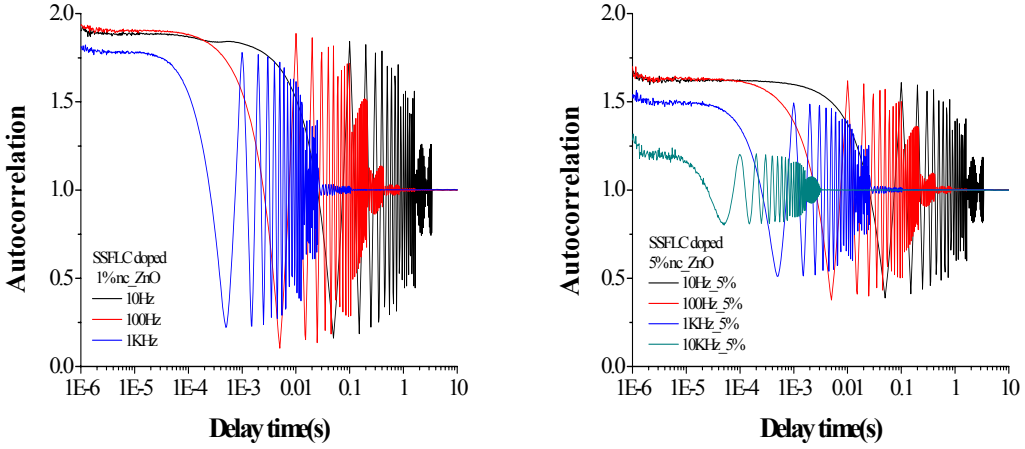

Figure 4-4-6(b): The corresponding autocorrelation function of SSFLC cells doped with 1 (left panel) and 5% (right panel), respectively.

The first thing one might notice is the oscillation behavior in the autocorrelation functions of SSFLC doped with 0.5%, and 5% nc-ZnO driven by an electric field with

frequency at 10 kHz. This oscillation that doesn't exist in pure SSFLC cell strongly implies that the doping effect truly enhances the dynamic electro-optic response. We attribute this enhancement to a faster response time, which is very likely to come from (1) zinc oxide nanoparticle itself has a giant permanent dipole moment, which is about 100 times larger than one FLC molecule [31]. There is no doubt that the coupling energy to the electric field would therefore increase and result in a faster response time of FLC according to eqn. (4.2.1); (2) in section 1.3.2, we knew that each of the FLC molecules possesses a spontaneous polarization due to the molecular chirality. However, for a bulk SmC* sample, free to develop its helical structure, will not show ferroelectric behavior since the spontaneous polarization will average to zero over one pitch. In brief, the macroscopic spontaneous polarization has everything to do with the alignment within the FLC cell; the better the alignment is, the stronger the macroscopic spontaneous polarization becomes. This conclusion indirectly confirms our deduction in chapter three which, through a mathematical description, tells us that the alignment of the FLC molecules is indeed improved by simply doping ZnO nanocrystals into the cell.

Another interesting observation from Fig. 4.4.2 is the amplitudes of oscillation in the ACFs of the four different SSFLC cell. The amplitude, according to conclusion (2), is an essential index that relates to the term $P_s E/\eta$, which governs the electro-optic

property. The quantitative relationship of amplitude among all the cells under study is listed in table 4.4.1.

Driving freq	Comparison of amplitude
10Hz	FLC+1%nz-ZnO > pure FLC ≒ FLC+0.5%nz-ZnO>FLC+5%nz-ZnO
100Hz	FLC+1%nz-ZnO > FLC+0.5%nz-ZnO>FLC+5%nz-ZnO>pure FLC
1 KHz	FLC+1%nz-ZnO > FLC+0.5%nz-ZnO>FLC+5%nz-ZnO>pure FLC
10 KHz	FLC+0.5%nz-ZnO>FLC+5%nz-ZnO>>pure FLC

Table 4-4-1: The quantitative relationship of amplitude.

From this comparison, we found that the amplitude in ACF is related to the alignment within the cell, for one can easily tell that the SSFLC cells doped with 0.5% and 1% nc-ZnO show greater amplitudes of oscillation than the pure one does at all frequencies. This observation corresponds to our conclusion in Chapter 3 that these two cells do have better alignment comparing to pure SSFLC, especially the one doped with 1% nc-ZnO, which also shows the best electro-optic property at field with frequency 10Hz, 100Hz, and 1 kHz. Another possible cause may come from a decrease in the thermal fluctuation within the SSFCL cells doped with 0.5% and 1% nc-ZnO. The simulation done in section 4.3 supports our theory that the more lightly the thermal force disturbs the deterministic field, the greater the autocorrelation value

will be reached. With these dynamic light scattering experiments, we are convinced that doping ferroelectric liquid crystals (FLC) with nanomaterials actually yields some degrees of freedom for tailoring FLC properties from various aspects. To be more specific, instead of synthesizing new mesogenic molecules to produce new LC materials with high application potentials, our approach of simply blending seems like a good way to go.

Chapter 5

Conclusion and Future Prospect

In this thesis, we attempt to discuss the dynamics of SSFLC. First, we start with the scattered light coming from the collective excitation induced by thermal energy inside the FLC molecules. This thermal fluctuation converted into autocorrelation function is then proved to be an indication of some material parameters that characterize the SSFLC system such as viscosity, elastic constant and temperature. The mathematical relation between thermodynamics and material properties enable us to examine the influence brought by doping nanocrystal ZnO into SSFLC from a macroscopic viewpoint and further confirm the fact that SSFLC shows better alignment with doping nc-ZnO. The experiment has once again proved that the thermodynamic is not just some random noise, but is full of useful information. However, the unpredictable dynamics become unwanted when controlling the material by applying external fields. It disturbs the deterministic path given by the field and lead to an unexpected output. This part of thermodynamics should be handled well or it would result in an unexpected error.

In addition to the industrial importance, liquid crystalline materials are interesting also as model systems for studying a broad spectrum of fundamental phenomena in physics due to the richness of different phases and the structures

analogous to many of the bio-system. For example, it may serve as a starting point for analysis of protein structure and evolution. The prospect of the bio-application of liquid crystal should be brightening.

References

[1] Toralf Scharf, Polarized Light in Liquid Crystals and Polymers, John Wiley & Sons, New Jersey, 2007.

[2] I. Musevic, R. Blinc and B. Zeks, the Physics of Ferroelectric and Antiferroelectric liquid crystals ,World Scientific, 2000.

[3] Peter J. Collings, "Ferroelectric Liquid Crystals: The 2004 Banjamin Franklin Medal in Physics presented to Robert B. Meyer of Brandeis University," J Franklin Institute, 342,599,205.

[4] R. K. Pathria, Statistical Mechanics, Oxford University Press, Oxford, 1972.

[5]F. Reif, "Fundamentals of Statistical and Thermal physics," McGraw-Hill Book Company.

[6] H. L. Pecseli, Fluctuations in Physical Systems, Cambridge University Press, 2000

[7] Kerson Hunag, Introdution to Statistical Physics, Taylor & Francis, London, 2001

[8] R. Kubo, "The fluctuation-dissipation theorem," Rep. Prog. Phys 29 255, 1966

[9]G. Barbero and L. R. Evangelista, "An elementary course on the continuum theory for nematic liquid crystals," World Scientific, Singapore, 2000.

[10] P. G. de Gennes and J. Prost, the physics of liquid crystals, Oxford University Press, Oxford, 1993.

[11]T. Akahane, K. Itoh and N. Nihei, "Dynamic Response of Surface-Stabilized Ferroelectric Liquid Crystals with Chevron Layer Structure," JJAP, 32, pp5041-5051, 1993.

[12] S. Ponti, M Becchi, and S. Torgova, " Bidimensional distortion in ferroelecetric liquid crystal with strong anchoring in bookshelf geometry," PRAMANA-journal of physics, 61, 2, 385, August 2003.

[13] S. Chandrasekhar, "Liquid Crystal," Cambridge University Press, 1992

[14] Bruce J. Berne and Robert Pecora, "Dynamic Light Scattering: With Application to Chemistry, Biology and Physics," Dover Publications, Mineola and New York, 2000.

[15] T. Wohland, R. Riglern and H. Vogel, "The Standard Deviation in Fluorescence Correlation Spectroscopy," Biophysical Journal vol.80, pp2987-2999, 2001

[16] M. J. Culbertson and D.L. Burden, "A Distributed Algorithm for Multi-Tau Autocorrelation," Review of Scientific Instruments, **78**, 044102, (2007)

[17] Luca Cipelletti and D. A, Weitz, "Ultralow-Angle Dynamic Light Scattering with A Charge Coupled Device Camera Based Multispeckle, Multitau Correlator," Rev. Sci. Instrum., 70 3214, August 1999

[18] Yu. Reznikov, O. Buchnev, O. Tereshchenko, V. Reshetnyak, A. Glushchenko, and J. West, "Ferroelectric Nematic Suspension," Applied Physics Letters, **82**, No 12, 1917-1919 (2003)

[19] C. I. Cheon, L. Li, A. Glushchenko and J. L. West, "Electro-optics of Liquid Crystals Doped with Ferroelectric Nano-Powder." SIDSymp. Dig. 45, 2, p1471 (2005)

[20] H.-Y. Chen, W. Lee, "Electro-Optical Characteristics of a Twisted Nematic Liquic-Crystal Cell Doped with Carbon Nanotubes in a DC Electric Field," Optical Review, **12**, 3, 223-225, (2005)

[21] Jung Y. Hunag, Liu S. Li, and Ming C. Chen, J. Phys. Chem. C **2008,** 112, 5410-5415

[22]E. Ouskova, O. Buchnev, V. Reshetnyak, Y. Reznikov and H. Kresse, "Dielectric relaxation spectroscopy of a nematic liquid crystal doped with ferroelectric Sn2P2S6 nanoparticles." *Liquid Crystals*, **30**[10], 1235-1239 (2003)

[23] D. J. Goyal, C. Agashe, M. G. Takwale, V. G. Bhide, S. Mahamuni, and S. K. Kulkarni, "Dopant induced modifications in the physical properties of sprayed ZnO:In films," *J. Mater. Res*., **8**, 1052 (1993)

[24] Yoshikawa H., Maeda K., Shiraishi Y., Xu J., Shiraki H., Toshima N. and Kobayashi S., "Frequency Modulation Response of a Tunable Birefringent Mode Nematic Liquid Crystal Electrooptic Device Fabricated by Doping Nanoparticles of Pd Covered with Liquid-Crystal Molecules." 41, pp 1315-1317, 2002

[25] Yuho Noguchi, Noriaki Ito, and Hirokazu Furue. "Fabrication of Defect-Free Surface-Stabilized Ferroelectric Liquid crystals Using Alignment Films Rubbed in Anti-Parallel," Taylor & Francis, London, 2008

[26] D. J. Goyal, C. Agashe, M. G. Takwale, V. G. Bhide, S. Mahamuni, and S. K. Kulkarni, *J. Mater. Res*., 8,1052 (1993)

[27] http://dasher.wustl.edu/bio5325/lectures/lecture-12.pdf

[28] E. Nelson."Dynamical theories of Brownian Motion," Princeton University Press, Priceton, New Jersey

[29] Singiresu S. Rao, "Mechanical Vibrations," Pearson Prentice Hall

[30] J.B. Bunning, T. E. Faber and P. L. Sherrell, J. Physique, 42 (1981), 1175-1182

[31] T. Nann and J. Schneider. *Chem. Phys. Lett.*, 384,150 (2004)

[32] L. Mikhaylovich Blinov," Electro-Optical and Magneto-Optical Properties of Liquid crystals," John Wiley & Sons Limited, Chichster, 1983.

[33] D. Demus, J. Goodby, G. W. Gray, H.-W. Spiss, and V. Vill, "Handbook of Liquid crystals," Wiley-VCH